OPTICAL MEMORY DEVELOPMENT

VOLUME I

Prototype Memory System

BY

L. S. COSENTINO, R. S. MEZRICH, E. M. NAGLE, W. C. STEWART AND F. S. WENDT

INTERIM REPORT

NOVEMBER 1972

PREPARED UNDER CONTRACT NAS8-26808

RCA LABORATORIES
PRINCETON, NEW JERSEY 08540

GEORGE C. MARSHALL SPACE FLIGHT CENTER
NATIONAL AERONAUTICS AND SPACE ADMINISTRATION
HUNTSVILLE, ALABAMA 35812

1. Report No.	2. Government Accession No.	3. Recipient's Catalog No.
Interim Report		

4. Title and Subtitle

OPTICAL MEMORY DEVELOPMENT

Vol. I Prototype Memory System

5. Report Date	
November 1972	
6. Performing Organization Code	

7. Author(s)	8. Performing Organization Report No.
L.S. Cosentino, R.S. Mezrich, E.M. Nagle, W.C. Stewart, F.S. Wendt	PRRL-72-CR-53

9. Performing Organization Name and Address	10. Work Unit No.
RCA Laboratories Princeton, New Jersey 08540	11. Contract or Grant No. NAS8-26808

12. Sponsoring Agency Name and Address	13. Type of Report and Period Covered
George C. Marshall Space Flight Center National Aeronautics and Space Administration Huntsville, Alabama 35812	Interim Report 3/12/71 to 10/17/72
	14. Sponsoring Agency Code

15. Supplementary Notes

16. Abstract

This report describes the design, development, and implementation of a prototype, partially populated, 10^6-bit read-write holographic memory system using state-of-the-art components. The system employs an argon ion laser, acoustooptic beam deflectors, a holographic beam splitter (hololens), a nematic liquid crystal page composer, a photoconductor-thermoplastic erasable storage medium, a silicon PIN photodiode array, with lenses and electronics of both conventional and custom design. Operation of the prototype memory system has been successfully demonstrated. Careful attention is given to the analysis from which the design criteria were developed. Specifications for the major components are listed, along with the details of their construction and performance. The primary conclusion resulting from this program is that the basic principles of read-write holographic memory system are well understood and are reducible to practice.

17. Key Words (Selected by Author(s))	18. Distribution Statement
Holographic memory Read-write system	

19. Security Classif. (of this report)	20. Security Classif. (of this page)	21. No. of Pages	22. Price*
Unclassified	Unclassified	73	

*For sale by National Technical Information Service, Springfield, Virginia 22151.

FOREWORD

This interim report, consisting of three volumes, was prepared by RCA Laboratories, Princeton, New Jersey, for the George C. Marshall Space Flight Center of the National Aeronautics and Space Administration, Huntsville, Alabama. It describes work done under Contract NAS8-26808 during the period from March 12, 1971 to October 17, 1972 in the Information Sciences Research Laboratory, Dr. Jan A. Rajchman, Staff Vice President and Director. The Project Supervisor was Mr. R. D. Lohman. Members of the Technical Staff who participated in the research reported in Volume I are Drs. W. C. Stewart and R. S. Mezrich and Messrs. L. S. Cosentino, F. S. Wendt, E. M. Nagle, and G. W. Leck. Messrs. C. W. Robbins, P. Mitnaul, J. L. O'Neill, D. Jose, J. A. Castellano, and R. N. Friel participated in the fabrication of devices and components used in the memory. The NASA Project Monitor was Mr. E. J. Reinbolt.

It should be noted that about 90% of the effort described in Volume I was supported by RCA Laboratories funds under its parallel research program and the remaining 10% was supported by contract funds.

Optical Memory System

TABLE OF CONTENTS

TABLE OF CONTENTS (Continued)

LIST OF ILLUSTRATIONS

LIST OF ILLUSTRATIONS (Continued)

TABLES

PROTOTYPE MEMORY SYSTEM

by

L. S. Cosentino, R. S. Mezrich, E. M. Nagle,
W. C. Stewart, and F. S. Wendt
RCA Laboratories
Princeton, New Jersey 08540

SUMMARY

This report describes the design, development, and implementation of a prototype, partially populated, 10^6-bit read-write holographic memory system using state-of-the-art components. The system employs an argon ion laser, acoustooptic beam deflectors, a holographic beam splitter (hololens), a nematic liquid crystal page composer, a photoconductor-thermoplastic erasable storage medium, a silicon PIN photodiode array, with lenses and electronics of both conventional and custom design. Operation of the prototype memory system has been successfully demonstrated. Careful attention is given to the analysis from which the design criteria were developed. Specifications for the major components are listed, along with the details of their construction and performance. The primary conclusion resulting from this program is that the basic principles of read-write holographic memory system are well understood and are reducible to practice.

I. INTRODUCTION

This report describes the design, development, and implementation of a prototype 10^6-bit holographic memory system. The principal purpose of the project was to determine that the basic concepts underlying large-capacity read-write holographic memories are realistic and realizable. Since practical light valve arrays and reversible storage media capable of operating in sub-millisecond cycle times with existing lasers remain to be developed, a complete system of non-trivial size that is capable of operating at realistic speeds as a computer memory cannot be built at present. The alternative approach taken here is to ignore the speed requirements for the moment, and to develop a system with the best presently realizable components. The original design employed a Q-switched ruby laser, a two-dimensional acoustooptic deflector, a liquid crystal page composer, a manganese-bismuth erasable magneto-optic storage medium, and a silicon photodiode detector array. Experimental difficulties with the ruby laser led to the substitution of an argon ion laser and a photoconductor-thermoplastic storage medium.

With the exception of laser power requirements, design of the system optics is essentially independent of the speed requirement. Following a brief description of the memory system, this report details the design analysis and then gives a complete description of each major system component.

The organization specified for the memory system is that there be space in the storage medium for at least 1024 holograms, each of which can store 1024 bits (one page) of information. To provide an extra margin of immunity to image fluctuations from a variety of possible sources, each bit of information in the image of a given page is associated with two diagonally adjacent resolvable spots, A and B. The condition A *on* and B *off* represents a binary "0", A *off* and B *on* represents a binary "1"; the two remaining combinations where A and B are simultaneously *off* or *on* are not used as inputs and represent an error condition if detected.

The memory system is partially populated in a manner which permits a realistic assessment of the performance of a fully populated system. The page composer is fully populated so that each page written into and read from a hologram contains the full 2048 resolvable points representing 1024 bits in a page. The deflection system has the full resolution for addressing any one of 1024 holograms. Only 48 of the possible hologram locations are active -- 16 in locations near the center of the array and 32 around the periphery. There are five separated groups containing four nearest neighbors so that full density in local areas at the center and boundaries is included. The photodetector array contains 20 diodes for sensing 10 of the 1024 bits in each image. These are divided among an adjacent bit pair at the center of the image and four bit pairs around the periphery of the image.

Other criteria are that the information packing density be reasonably high ($\geq 10^3$ bits/mm^2), that light utilization be efficient, and that the basic design be capable of extension to larger

sizes and higher capacities. Figure 1 is top-view sketch of the holographic optical system layout selected for the system. The remainder of this section summarizes the function of the components.

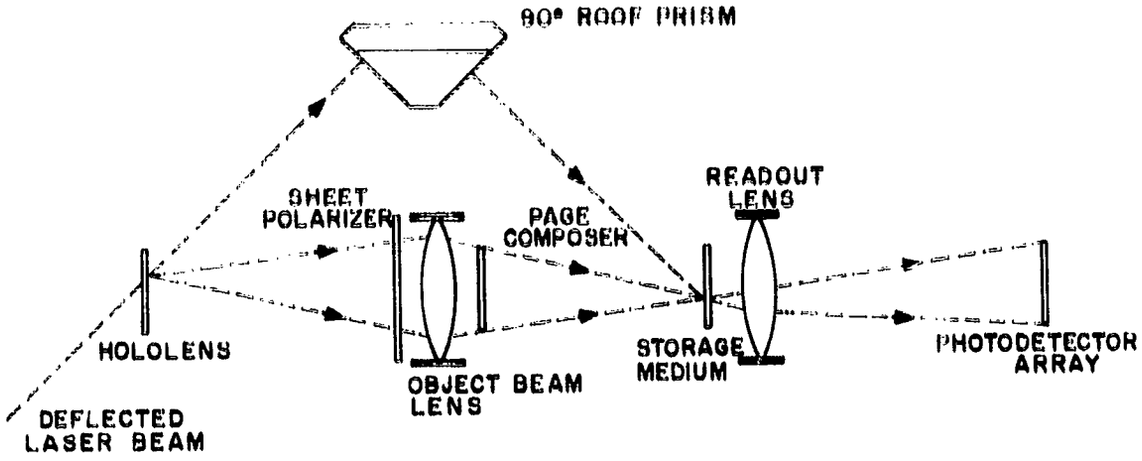

Figure 1. Holographic optical system.

The light input to the system is a small collimated and polarized laser beam which intercepts the hololens at a fixed angle, 45° here. The point of intersection is selected by a deflection system, not shown, which is capable of displacing the beam parallel to itself both horizontally and vertically in fixed increments. Each possible position of the beam will ultimately result in the illumination of a single hologram location on the erasable storage medium. The hololens consists of an area array of permanently prerecorded holograms, one for each page of memory capacity. Light diffracted by the hololens, when polarized parallel to the transmission axis of the sheet polarizer, passes through the object beam lens to illuminate the light valves of the page composer. The object beam lens projects an image of the illuminated hololens area onto the storage medium. Thus, the object beam light from the page composer strikes the storage medium only at the location where a hologram is to be written. The page composer is a two-dimensional array of light valves. The transmission of each light valve is controlled by electrical signals which compose the page of information to be recorded in a hologram on the storage medium. Since the active area of the page composer containing the light valve array is the aperture stop for the object beam lens, the array has an approximately circular boundary in order to minimize the required lens diameter.

The zero-order component of the collimated input light beam, which is not diffracted by the hololens but is transmitted without deviation, is folded by a 90° roof prism and arrives at the storage medium at a horizontal offset angle of 45°. This beam is used as the reference wave for recording holograms on the storage medium. Two reflections inside the prism produce inversion of the horizontal and vertical positions of the reference beam which match the inverted

image of the hololens produced by the object beam lens. Thus, object and reference beams are coincident on the storage medium for any point of incidence of the input beam on the hololens.

Storage medium holograms are read out by rotating the plane of polarization of the input beam by 90°. Diffracted light from the hololens is blocked by the sheet polarizer, so that only the reference wave illuminates the selected hologram on the storage medium. The reconstructed wavefront represents a virtual image of the page composer in the state of transmission which existed during the recording of the hologram. This image is projected at unity magnification onto the photodetector array by the readout lens; it is diffraction limited by the small aperture of the single hologram which is read out at any given time. Since there can be no vignetting of the image rays from any of the holograms arrayed on the storage medium, the active storage medium area forms the aperture stop for the readout lens. The boundary of this area is also made approximately circular. The photodetector array contains a photosensitive diode at each location where the image of a page composer light valve can appear. The information output of the system consists of the resulting electrical signals.

In summary, the principal advantages of the present optical configuration are:

(a) Storage medium holograms of high packing density are recorded in the Fourier transform plane of the page composer.

(b) Use of the hololens provides deflection for the object beam with efficient light utilization for writing.

(c) Locating the page composer and erasable storage medium adjacent to the imaging lenses minimizes the lens diameters for given focal lengths and memory capacity.

(d) Use of the same reference beam incidence angles for both writing and reading permits alignment of the photodetector array without recording holograms.

The principal disadvantages are:

(a) The object illumination must be blocked during readout.

(b) Different increments of horizontal and vertical displacement of the deflected input beams arriving obliquely at the hololens must be provided.

II. OPTICAL SYSTEM DESIGN

A specification of parameters such as size or spacing for one component in the optical system usually dictates requirements for other components. In this section, some of the important relationships among the components are analyzed. Simplifying approximations and empirical measurements are used freely. The purpose is to provide a semiquantitative basis for evaluating tradeoffs in arriving at a final design.

A. Deflector Resolution

The number of resolvable positions N in one dimension that is obtained from an acousto-optic deflector cell is given by

$$N = \Delta\theta / \Delta\phi \tag{1}$$

where $\Delta\theta$ is the angular range over which the incident laser beam can be deflected (assuming small deflection angles), and $\Delta\phi$ is the incremental angular spacing between the central rays of two adjacent deflected beams. The far-field diffraction pattern, appearing in the back focal plane of a lens, contains the spatially resolved light spots. The angular range depends on the frequency range of the acoustic waves, the light wavelength λ, and other constants. The allowable angular spacing $\Delta\phi$ depends on the amount of diffraction spreading of the light due to the finite diameter D of the cell's optical aperture, and the amount of overlapping of spots which can be tolerated. Since the diffraction spread is proportional to λ/D, let

$$\Delta\phi = \alpha\lambda/D, \tag{2}$$

where the constant of proportionality α is chosen according to the desired resolution criterion. For a uniformly illuminated aperture and an effective Rayleigh resolution criterion in which spots are considered resolved when the maximum of one spot falls on the first minimum of the neighboring spot, $a = 1.22$ and

$$N(\text{Rayleigh}) = \Delta\theta\ D/1.22\lambda \tag{3}$$

Since the input laser beam has an inherent Gaussian intensity profile through its cross section, only 37% of the light power can be utilized in forming a perfectly uniform beam. If a sufficiently small-diameter Gaussian beam is used such that substantially no light is blocked by the cell aperture, the increased diffraction spreading reduces the number of spots resolved according to a given criterion and for a fixed aperture size. A useful compromise for optimizing light throughput and resolution is to expand the laser beam so that the cell aperture truncates the laser beam at its $1/e^2$ intensity radius. This allows 86% of the laser beam through the aperture, and increases the diffraction spreading to approximately 1.4 times the value obtained with no truncation of the same size Gaussian beam. Let $\Delta\beta$ represent the angular spread over which the output beam drops from its central maximum to 1/e of this intensity value. It can

be shown that

$$\Delta\beta = 0.672\ \lambda/D \tag{4}$$

For a resolution criterion that specifies the separation between centers of neighboring spots be k times $\Delta\beta$,

$$\phi = 0.672\ k\ \lambda/D \tag{5}$$

and

$$\alpha(k) = 0.672\ k \tag{6}$$

Therefore, for a given λ and D, the number of resolvable spots N_k according to the above criterion can be expressed in terms of the number resolved by the Rayleigh criterion:

$$N_k = N(\text{Rayleigh}) \times 1.82/k \tag{7}$$

It can be seen that as k increases, the Rayleigh resolution of the deflector must increase in order to obtain a given number of spots resolved by the k criterion.

B. Reference Beam Spreading

A major influence on image contrast arises from the partial illumination of neighboring holograms on the storage medium during readout of a particular addressed hologram. The reference beam (and the object beam) must have sufficient extent to properly expose the storage medium during writing to produce a hologram of the desired diameter. During readout, when the reference beam is centered on the addressed hologram, the total light flux onto the neighboring holograms must be significantly less than on the selected hologram. Illumination of the deflector aperture with a Gaussian beam profile which is truncated at the $1/e^2$ intensity radius results in a deflected beam profile that is very nearly Gaussian in the main lobe. This profile is therefore approximated by the expression

$$I(r) = I_o \exp\left[-(r/r_o)^2\right] \tag{8}$$

where r is the radial coordinate in the storage medium plane, centered at the addressed hologram, and r_o is the radius at which the intensity falls to 1/e times the central intensity I_o.

Assume that the efficiency with which the image of each data spot is reconstructed at the photoconductor is the same for each hologram in the array. The images from neighboring holograms that are partially illuminated are derived from the same coherent wavefronts of the reference beam that produce the desired image. The images from the neighboring holograms arrive at the photodetectors at slightly different angles, however, and produce spatial interference patterns whose periods are smaller than each photodetector. The result is that it is necessary to add the respective intensities of the illumination from neighboring holograms, rather than the

amplitudes, because of the spatial integration which occurs over the area of each photodetector. The question of interest is thus reduced to consideration of the light flux on the addressed hologram compared with the total from all the neighbors.

Define F_a as the fraction of the total light flux in the reference beam which falls within the boundary of the addressed hologram. Similarly, F_n is the total light flux on neighboring holograms, expressed as a fraction of the total incident flux. The minimum contrast C_r in the image due to readout beam spreading is

$$C_r = F_a/F_n \tag{9}$$

For square holograms of width h, in a two-dimensional square array with center-to-center spacing s_h, define the one-dimensional packing factor η_h as

$$\eta_h = h/s_h \tag{10}$$

The quantity k is given by

$$k = s_h/r_o \tag{11}$$

Figure 2 is a graph of the results of a numerical computation of the dependence of C_r on η_h for various values of k. Figure 3 plots the dependence of F_a on these parameters. Whereas F_a increases as both η_h and k increase, C_r increases with decreasing η_h and increasing k. Using circular holograms of diameter h is equivalent to reducing η_h by a small amount in these calculations. Further discussion of the choice of parameter values will appear in a later section.

C. Image Resolution

Consider the diffraction spreading in the image caused by a finite hologram diameter h. The page composer is illuminated by coherent light of wavelength λ which is converging to a point in the Fourier transform plane at an axial distance z from the page composer. Page composer light valves of diameter p form a periodic array with center-to-center spacings of s_p. Over 80% of the light transmitted by the page composer appears in a circle of diameter d_A in the Fourier plane; this is the size of the central disc in the Airy diffraction pattern of one light valve.

$$d_A = 2.44\,\lambda z/p \tag{12}$$

Experimental measurements were used to determine the dependence of diffraction-limited image contrast on the quantities

$$a = h/d_A \tag{13}$$

and

$$\eta_p = p/s_p \tag{14}$$

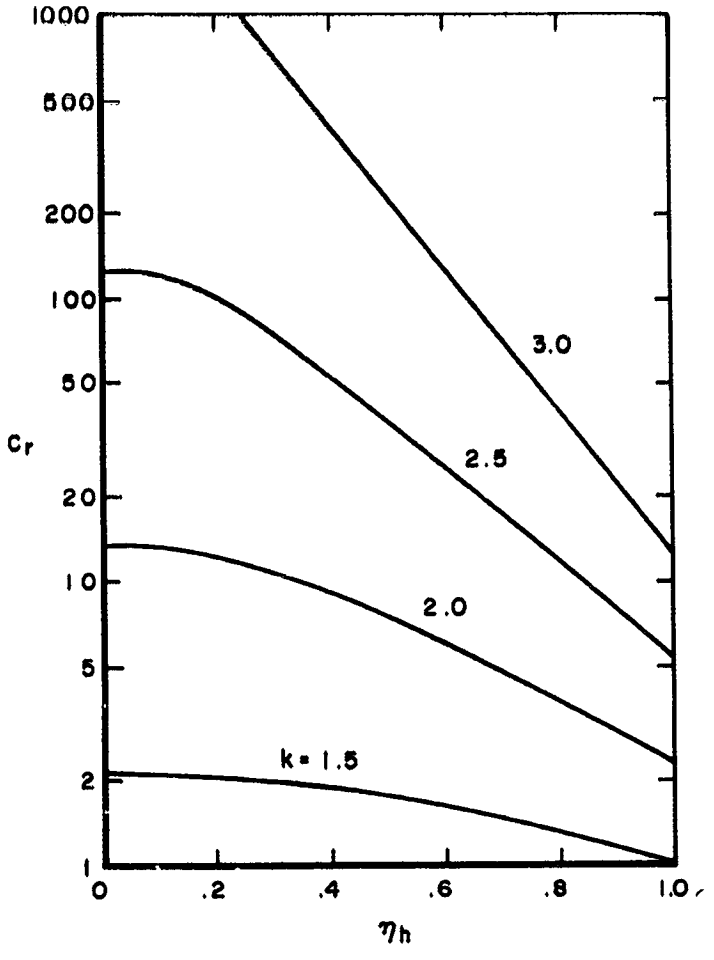

Figure 2. Worst-case image contrast due to reference beam spreading as a function of hologram size and spacing.

A sketch of the experimental setup is shown in Fig. 4. Collimated laser light is incident on a metal mask with periodic apertures which simulate the elements of the page composer. In the back focal plane of the lens, the light intensity distribution is the Fourier power spectrum of the amplitude transmittance of the page composer mask -- this is the plane in which a hologram would be formed to give maximum information density. In this arrangement, the effective value of z is the lens focal length f. Further down the light path is the real image of the page composer projected by the lens, given by the condition $x\,x' = f^2$. A circular aperture representing the hologram aperture was placed in the Fourier transform plane to transmit only the light wavefronts which could be reconstructed from a hologram of the same size. A photodetector was placed in the image plane with an entrance aperture equal in size to that of the projected image of one page composer element.

In the experiments, measurements were made of the light flux collected by the photodetector in the image of one opaque page composer element surrounded by all transparent elements, and the light flux in the image of an adjacent transparent page composer element. The ratio of

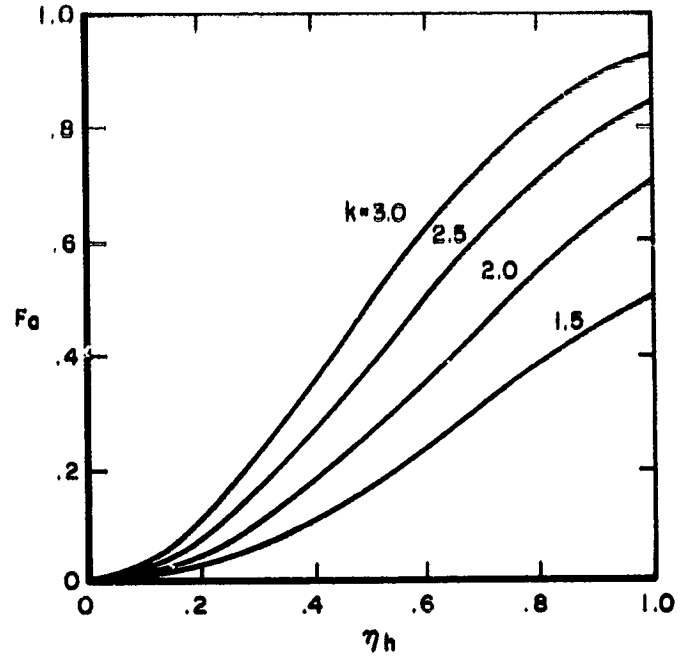

Figure 3. Fraction of reference beam light flux on addressed hologram as a function of hologram size and spacing.

light in the image of a transparent element to that in the opaque element is called the diffraction-limited contrast C_d; it was determined for a range of values of a and η_p. Ratios as high as 4 x 10^4 could be measured without serious error from flare light in the system. The results may be applied to a system with other scaling factors such as lens focal length, magnification, page composer size, etc., by maintaining the same ratio a between hologram aperture diameter and the

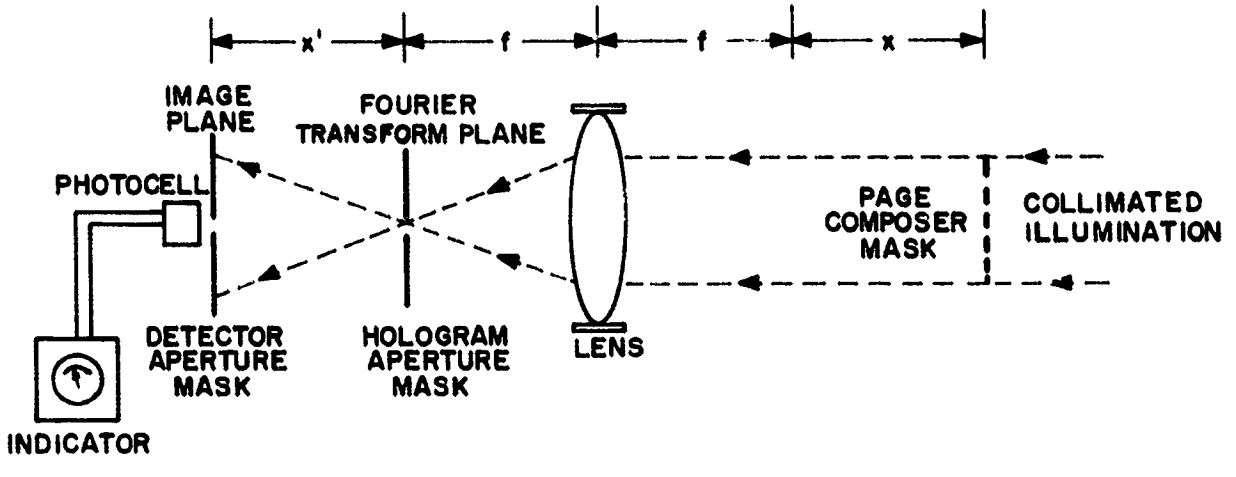

Figure 4. Experimental setup to measure diffraction-limited contrast.

diameter of the central Airy disc in the Fourier transform (far-field diffraction pattern) of a single page composer element. A portion of the experimental data is listed in Table I below.

Table I

Experimentally Measured Values of Diffraction-Limited Contrast C_d as a Function of a and η_p

η_p \ a	1.7	1.5	1.4	1.2	1.0	0.8	0.65	0.5
0.40	10,700	3980	1430	1070	15,000	2640	415	111
0.50	2210	3240	872	2440	2600	1730	420	2880
0.67	711	600	814	425	1920	179	260	2.65
0.75	--	--	--	206	1030	100	4.7	--

The fluctuation of C_d as a varies is a real effect caused by the abrupt boundary of the hologram aperture in the experiments. Note that C_d is greater than 10^2 over a ±20% variation in hologram diameter around the value $a = 1$ for all the experimental values of η_p.

An additional insensitivity to the effects of diffraction spreading is built into the geometrical arrangement of image points which constitute an information bit. Diagonally adjacent pairs of detectors represent a single information bit; the pairing of neighboring spots into bits is such that the spillover light, from any valid combination of information states in the neighboring spots, falls equally on the two detectors. The desired information forms a difference mode signal, while the noise due to diffraction spreading becomes common mode. The effective contrast from diffraction spreading becomes the product of C_d as measured for single spot detection and the common mode rejection ratio of the detector electronics. Defects which alter the effective hologram aperture into a nonsymmetric shape, however, will tend to degrade the contrast in both factors. Since the value of η_p influences other parameters in the design, discussion of the final choice is deferred to a later section.

D. Other Considerations

Another aspect of image contrast to be considered is the extinction ratio required of the sheet polarizer used to block the object illumination during readout. The sheet is aligned to transmit the vertically polarized object illumination during writing; the intensity transmittance is m_1. Transmittance of the horizontally polarized object illumination during readout is m_2, where $m_2 \leq m_1$. If the light flux from one page composer bit is F_o at the hologram during writing, then the flux into the image of a bit due to unextinguished direct object illumination is $F_o \tau m_2/m_1$, where τ is the intensity transmittance of the storage medium. The light flux in the image of a bit reconstructed from the stored hologram is the product of the reference beam flux F_a, and the efficiency e per bit. Define

$$K = F_a/F_o \tag{15}$$

and note that the reference beam flux at the hologram is the same for both reading and writing. The contrast C_p is the ratio of the flux in the readout image of a bit to the flux from unextinguished direct object illumination.

$$C_p = Kem_1/\tau m_2 \tag{16}$$

Intermodulation distortion, in Fourier-transform hologram images of a periodic object such as the page composer, reduces contrast by producing secondary images of an illuminated spot at the primary image locations of other page composer elements. The effect occurs when the reconstructed wave amplitude is not linearly proportional to the object wave amplitude used in recording the hologram. Spatial fluctuations of the object beam amplitude which are sufficiently large to exceed the linear dynamic range of the recording medium produce a recorded nonlinearity. Pseudo-random phase plates which uniformly shift the phase of the optical wavefront from each page composer element greatly reduce the spatial fluctuations. An alternative is to use diffuse illumination of the page composer at the expense of introducing speckle noise in the image from a high-density hologram. Nonlinear distortion is also inherent in the reconstruction of linearly recorded phase holograms of high efficiency; however, this effect is essentially negligible for peak diffraction efficiencies less than approximately 10%.

E. Storage Capacity

This portion of the analysis defines the influence of storage capacity on the design parameters. The following quantities are defined:

N_p - number of page composer elements

N_s - number of holograms in the storage medium

p - diameter of one page composer element

h - diameter of one hologram in the storage medium

s_p - center-to-center spacing of page composer elements

s_h - center-to-center spacing of holograms

η_p - spatial one-dimensional duty factor of the page composer $\equiv p/s_p$

η_h - spatial one-dimensional duty factor of the hologram array $= h/s_h$

A_p - required area of the page composer, including space between elements

A_s - required area of the storage medium, including space between holograms

P - diameter of the circle superscribed around the required page composer area

S – diameter of the circle superscribed around the required storage medium area

λ – wavelength of light used for writing and reading

f – focal length of object beam and readout image lenses

z – axial distance from page composer to storage medium

a – ratio of hologram diameter h to the diameter of the central Airy disc in the Fourier transform pattern of one page composer element

$\#$ – effective f/number of the imaging lens system = z/P

Since the page composer elements and the storage medium holograms each form a square array,

$$A_p = N_p(S_p)^2 = N_p(p/\eta_p)^2 \tag{17}$$

$$A_s = N_s(S_h)^2 = N_s(h/\eta_s)^2 \tag{18}$$

The hologram diameter is a times the diameter of the Airy disc of a page composer element,

$$h = 2.44\, a\lambda z/p \tag{19}$$

Combining Eqs. (17), (18), and (19) gives

$$A_pA_s = N_pN_h(2.44\, a\lambda z/\eta_p\eta_h)^2 \tag{20}$$

Choosing the boundaries around the page composer elements and the storage medium hologram array to be octagonal rather than square gives

$$A_p = \sqrt{2}\, p^2 \tag{21}$$

and

$$A_s = \sqrt{2}\, S^2 \tag{22}$$

Combining Eqs. (21) and (22) with (20) gives

$$2p^2S^2 = N_pN_h(2.44\, a\lambda z/\eta_p\eta_h)^2 \tag{23}$$

F. Specifications

To fix the design of the optical system requires numerical specification of eight quantities: hologram diameter and spacing, light valve diameter and spacing, wavelength, axial separation between page composer and storage medium, resolution criterion for deflector, and photodetector diode diameter. To maximize the readout light, the diameter of the photodetector is chosen to equal the diameter of a page composer light valve. In order to obtain identical specifications for

focal length and aperture of the object beam lens and the readout lens, the page composer diameter P is set equal to the storage medium diameter S. This choice also minimizes the range of angles over which the object beam is incident on the storage medium. The 1024 holograms in the storage medium are arranged as a 36 x 36 square array with the corners truncated to give an octogonal boundary, requiring a deflector resolution of 36 positions in each dimension instead of 32. The remaining parameter values were chosen to give reasonable trade-offs between image contrast on the one hand, and practical size and cost on the other hand.

Table II lists the resulting specifications. The initial design was for a ruby laser system incorporating a MnBi storage medium. The specific Curie-point writing characteristics of the MnBi limit the information recording density and are an important consideration in this design. A calculated worst-case image contrast of approximately 5:1 results in equal parts from reference beam spreading and from the 100:1 polarization extinction ratio in the object beam. Construction of the system components was begun on the basis of this initial design.

Table II

Design and Performance Specifications

Parameter	Initial Design	Final Design
λ (nm)	694.3	488.0
a	1	2.3
k	2	2
z (mm)	356	356
#	5	5
h (mm)	0.64	1.0
s_h (mm)	1.9	1.6
η_h	0.33	0.64
S (mm)	71	58
p (mm)	0.97	0.97
s_p (mm)	1.3	1.3
η_p	0.75	0.75
P (mm)	71	71
N(Rayleigh)	40	40
e	10^{-4}	10^{-2}
K	10^2	10
τ	0.1	1
m_1/m_2	100	100
C_d	10^3	$> 10^4$
C_r	10	6
C_p	10	10

The final design resulted from a decision to change to an argon laser and a photoconductor-thermoplastic storage medium. Since the available hologram diameter is determined by the size of a resistance heater in the photoconductor-thermoplastic device, a higher packing density of holograms on the storage medium is achievable. The final design was based for practical reasons on minimizing changes in the components that were already specified in the initial design; the deflector cells, page composer size, and lens focal lengths are left unchanged. Since the active storage medium diameter is smaller than in the initial design, and the holograms are larger than necessary for diffraction-limited imaging, the final design is not optimum. A seven- to eight-fold increase in the number of page composer elements would be allowable under the image contrast constraints used in the initial design.

III. LASER BEAM DEFLECTION SYSTEM

A. Deflector Cells

The holographic optical system design requires that the deflector cells resolve 36 positions with the center of an adjacent spot falling at twice the e^{-1} intensity radius of an addressed spot. The cells are illuminated with an expanded and collimated laser beam which is truncated at the e^{-2} intensity radius by the cell aperture. These requirements are equivalent to specifying a cell capable of resolving 40 positions according to the usual Rayleigh criterion for uniform incident illumination. Two lead molybdate deflector cells (Isomet Corporation, modified model 1101), having a specified maximum Rayleigh resolution of 42 positions, and associated drivers were purchased. Other specifications are (a) bandwidth ~ 29 MHz centered at 91 MHz, (b) angular deflection range across bandwidth ~ 4 milliradians, (c) diffraction efficiency per cell across bandwidth ~ 60%, (d) access time 1.75 μsec, (e) optical aperture ~ 6.3 mm, and (f) spot position accuracy ~ 1/8 spot separation at 20% operating duty cycle.

B. Deflector Telescope

The laser beam, which may be deflected over an angular range $\Delta\theta$ of 4×10^{-3} radian by the deflector cell, is to be converted by a lens system into small collimated beams parallel to the optical axis which can span the 55-mm width of the active areas of the hololens and storage medium. Placement of the deflector cell in the front focal plane of a lens system with an effective focal length f' provides, in the back focal plane, a span y given by

$$y = f'\Delta\theta \tag{24}$$

for small values of angular range. This requires f' to be 13.7 m. With the given deflector cell aperture and this focal length, the diameter of the output beam changes less than 5% over an axial distance of 2 m centered on the output plane. Thus, the deflected beams are parallel and effectively collimated at the hololens plane and the storage medium plane, which are separated by an axial distance of 1 m.

Shifting the deflector cell axially away from the front focal plane of the lens affects the parallelism of the deflected beams arriving at the back focal plane; the deviation from normal incidence of the arriving beams is greatest at the extremes of the angular range, and is zero at the center of the angular range. It can be shown for an axial translation d of the deflector cell from the front focal plane, that the beam leaving the deflector cell at an angle ϕ measured from the center of the angular deflection range will arrive at an angle δ

$$\delta = d\phi/f' \tag{25}$$

in the back focal plane, but at the same position in the plane as when d is zero. Our requirement is that a deflected beam arriving at a point on the hololens arrive at the equivalent point obtained by

parallel projection onto the storage medium with an error of no more than one-fourth the diameter of one hologram. Using the design values of 1-mm hologram diameter and 1-m axial distance between hololens and storage medium, the maximum allowable angular deviation δ_{max} from parallelism is

$$\delta_{max} = 0.25 \times 10^{-3} \text{ radian} \tag{26}$$

Substituting this value along with $\phi = 2 \times 10^{-3}$ radian and the value of f' gives the maximum allowable axial displacement d_{max} of the deflector cell from the front focal plane of the lens:

$$d_{max} = \delta_{max} f'/\phi = 1.7 \text{ m} \tag{27}$$

This comfortably large tolerance results primarily from the small range of deflection angles involved.

The system of three lenses spaced as shown in Fig. 5 is equivalent to a single lens having an effective focal length of $f_3 f_5 / f_4$; the distance between front and back focal planes is $2(f_1 + f_2 + f_3)$.

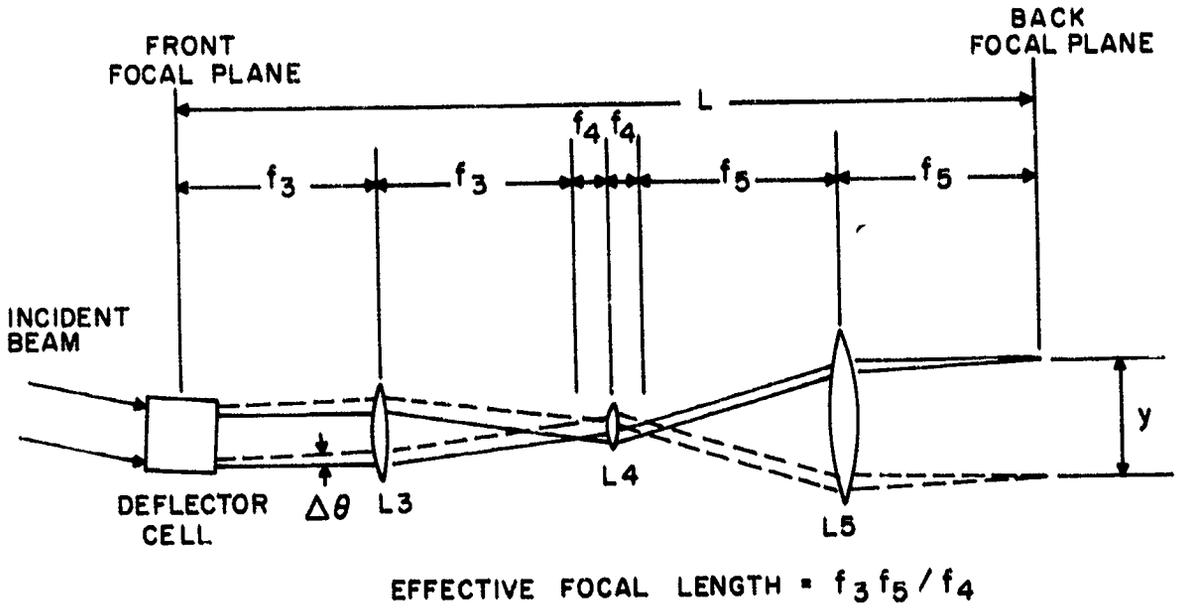

Figure 5. Compact lens system.

For a given effective focal length, this distance is minimized by choosing $f_3 = f_5$, and making f_4 as small as possible. In the back focal plane of lens 3 is the far-field diffraction pattern of the deflector cell as previously discussed. The size of the pattern is too small to be used directly since f_3 alone is much smaller than the required effective focal length. The back focal plane of lens 4 contains an image of the deflector cell with the transverse dimensions magnified by the ratio f_4/f_3 (much less than unity), but with all beam angles magnified by f_3/f_4. Lens 5 produces in its back focal plane the far-field diffraction patterns of the image located in its front focal plane. Equivalently, the pattern

at the back focal plane of lens 5 is an image of the diffraction pattern in the back focal plane of lens 3, magnified in transverse dimensions by the ratio f_5/f_4 (greater than unity), and with beam angles magnified by f_4/f_5. This system has the same tolerance to axial displacements from the input and output planes as calculated for the single lens to which it is equivalent.

The memory system design requires that the hololens and storage medium planes be inclined at an angle of 45° in the horizontal plane to the parallel beams arriving from the deflection system. The total lateral span, x, for the x-axis deflector, and the effective focal length of the optical system in the horizontal dimension must be smaller than the values for the vertical dimension by the factor cos (45°). The resolution of the x-deflector must be the same as the y-deflector, however. The effective focal length f_h of the lens system for horizontal deflection from Eq. (24) is

$$x = y \cos(45°) = f_h \theta \tag{28}$$

or

$$f_h = 9.7 \text{ m} \tag{29}$$

A lens configuration which satisfies the requirements is sketched in Fig. 6. The expanded laser beams first enter the y-deflector cell, which produces vertical deflection with a 4×10^{-3} radian angular range. Lens 1 and lens 2 are cylindrical lenses with refractive power only in the vertical dimension. The cylindrical telescope images the aperture of the y-deflector cell onto the x-deflector cell with a

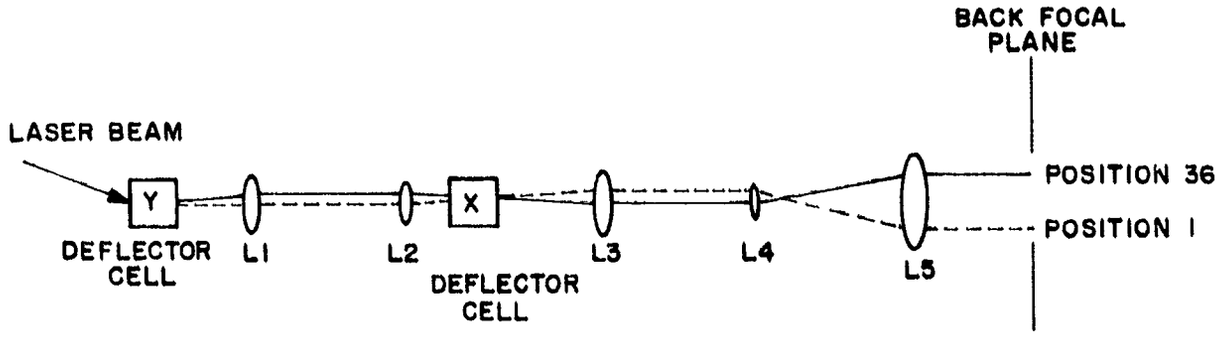

Figure 6. Deflector lens system.

transverse magnification of f_2/f_1, and an angular range magnification of $f_1/f_2 = 1.41$. The diffraction spreading in the horizontal direction between the two cells is negligible. The deflected beams exiting from the x-deflector cell have a horizontal angular range of 4×10^{-3} radian; the effective center of deflection for both dimensions lies at the x-deflector cell. A three-lens spherical telescope with an effective focal length of 9.7 m thus provides the proper rectangular format of deflected, collimated beams near the back focal plane of the system.

Design values chosen for the deflector optics are:

f_1 (cylinder)	–	141.4 mm
f_2 (cylinder)	–	100 mm
f_3	–	200 mm
f_4	–	12.7 mm
f_5	–	300 mm

Lenses L3 and L5 have a relative aperture of f/5 and are corrected for spherical aberration. Lenses L1, L2, and L4 are of plano-convex simple form, stopped down to relative aperture values from f/10 to f/20. The overall axial separation from the first deflector cell to the output plane is 1.9 m.

C. Deflector Performance

The overall efficiency of the deflector telescope, including the initial beam expander and truncation aperture, is 70%. The efficiency of the cascaded deflector cells above, when operated at nominal drive power, is 20%. Striations of inhomogeneous refractive index in the lead molybdate crystals produce the most serious limitation to deflector performance. These imperfections produce wavefront aberrations of greater than one-half wave and distort the far-field diffraction pattern of a deflected spot.

Figure 7(a) shows an enlarged photograph of the light distribution in the output plane of the deflector telescope when the deflector cells are removed. This distribution, for which the central disc is overexposed here, is the diffraction pattern resulting from the truncation aperture. Figure 7(b) is a photograph of the output plane with the same exposure as (a), after the deflector cells are inserted. The central lobe is distorted, the side lobes are much stronger, and the striations produce additional preferential scattering in the horizontal and vertical directions. Measurements show that the aberrations alone spread the light distribution to approximately 1.5 times the intended extent. Thus, there is relatively less light flux at the addressed hologram and more spillover light at the neighboring holograms. Figure 7(c) is a photograph of the output plane, without overexposure, showing the deflected spots resulting from scanning all combinations of positions 1, 2, 13, 18, 19, 24, 35, and 36 for x- and y-deflection. With the exception of 16 spots, 4 in each corner, this pattern represents the spatial locations of the 48 active holograms in the storage medium.

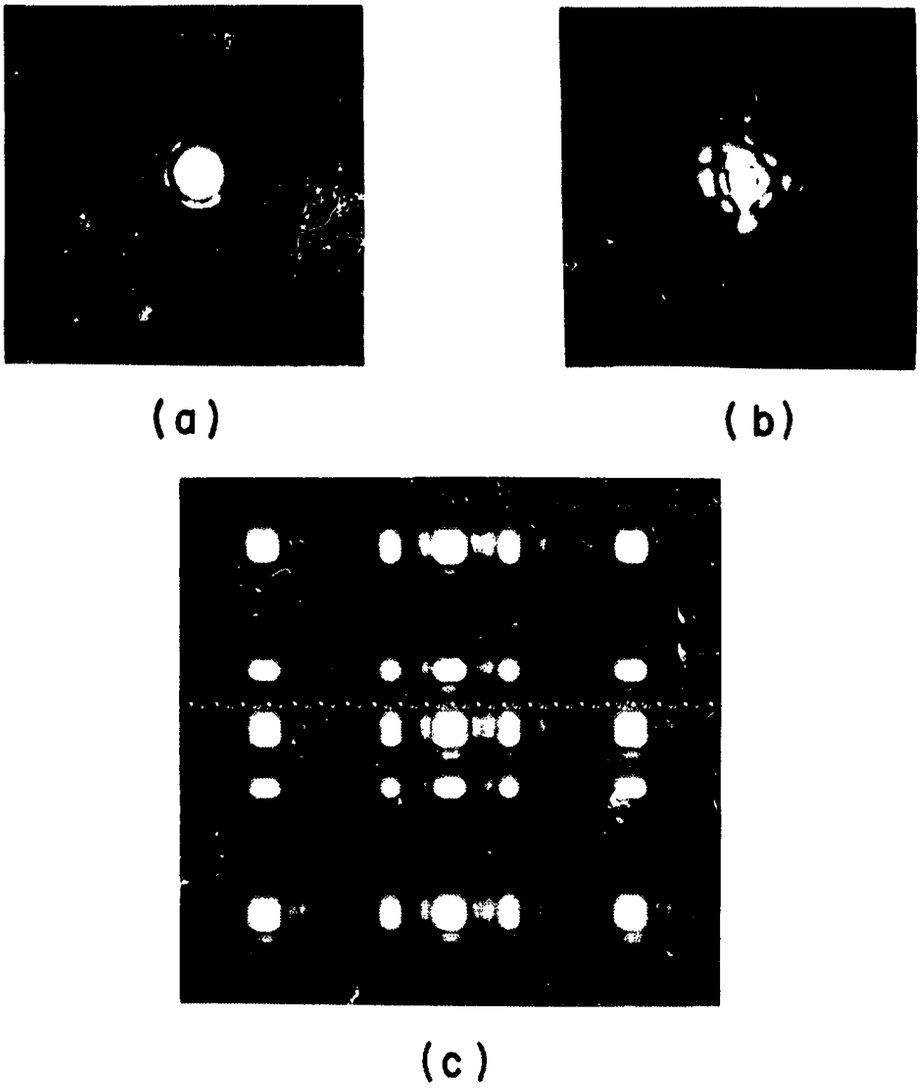

Figure 7. Output plane of deflector telescope, 1:1 scale.
(a) Without deflector cells; central spot is overexposed. (b) With deflector cells; same exposure as (a). (c) Scanning all positions sequentially; normal exposure.

IV. OTHER OPTICAL COMPONENTS

A. Hololens

The hololens is an array of permanent phase holograms which serves as the beam splitter for recording holograms in the erasable storage medium. Diffracted light from the hololens is used to illuminate all the light valves of the page composer. The hololens holograms represent blank pages of information; these holograms are copied onto the erasable storage medium with the page composer providing the desired information pattern.

Simultaneous recording of the entire hololens array is accomplished with the geometry sketched in Fig. 8. The page composer mask is a metal sheet with clear openings etched in the locations of the

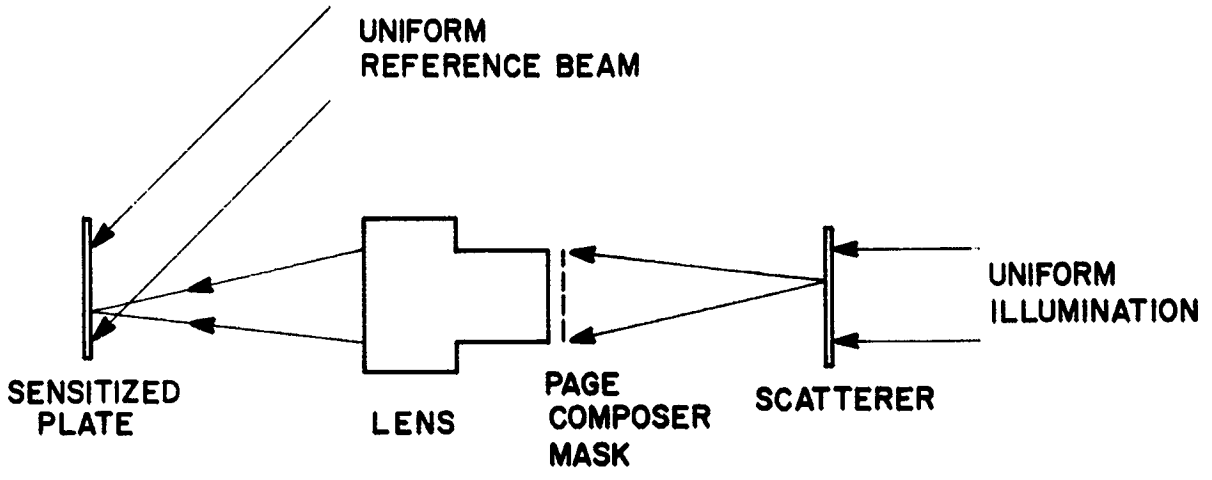

Figure 8. Hololens recording geometry.

page composer light valves. A random phase plate is also included with the mask to uniformly shift the phase of each aperture according to a computer-generated pseudo-random sequence. Randomization of the phases ensures a sufficiently uniform spatial distribution of object illumination at the holograms. The optical element denoted as the scatterer is imaged by the lens onto the sensitized dichromated gelatin plate which will become the hololens array. Uniform illumination of the page composer mask must be provided by each discrete scatterer point that is imaged onto a hologram location in the hololens array. One such point is depicted in the figure. A uniform collimated beam incident at 45° to the sensitized plate provides the reference wave for simultaneously recording the entire hololens array.

In order to provide uniform, spatially coherent illumination of the page composer, the scatterer consists of a multiple lens array. Focussed spots of light, one for each lenslet of the scatterer, are simultaneously imaged onto the sensitized plate at each point where a hologram is to be recorded. Molded plastic lens arrays would appear to be ideally suited for this purpose. Our observations have shown, however, that the surface finish of such arrays is generally too poor to give a uniform cone of

illumination with coherent light. The results shown here are obtained with individually selected and mounted simple glass lenses. Figure 9(a) is a photographic image of the page composer mask

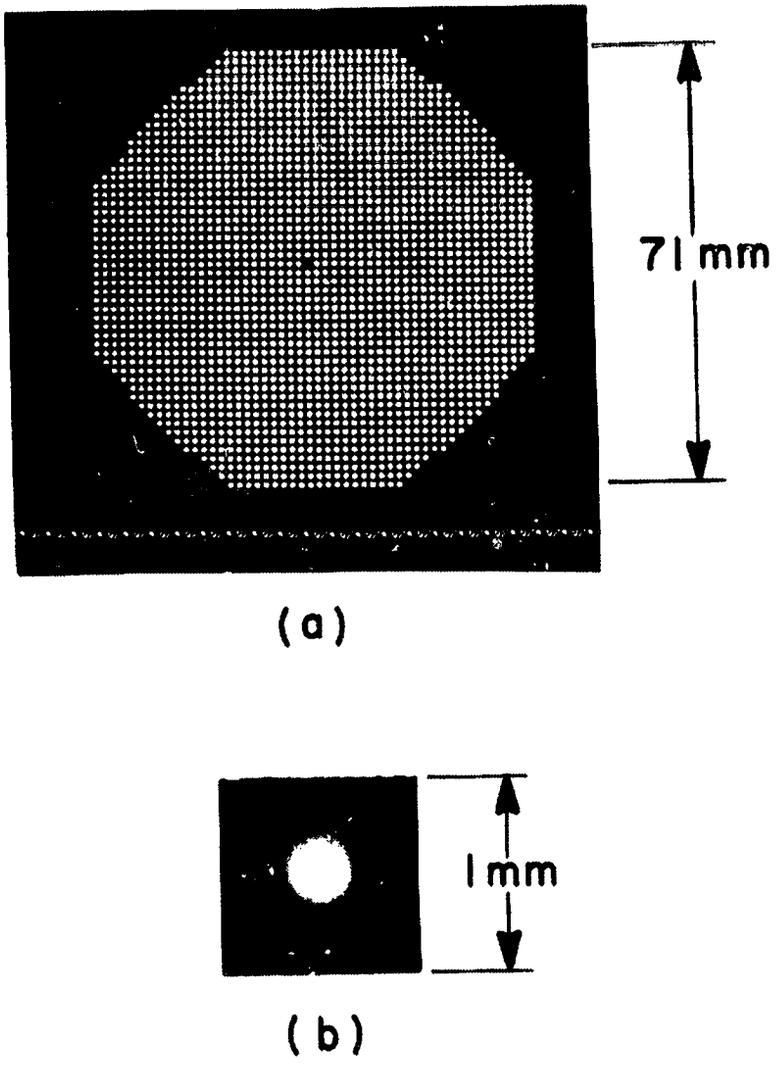

Figure 9. (a) Image of page composer mask, illuminated by one lenslet, as seen through 1-mm hologram aperture. (b) Object illumination of one hologram in hololens array.

taken through the 1-mm aperture of one hologram in the hololens plane. The opaque aperture near the center is deliberately introduced. The illuminating lenslet in this case has a slight cosmetic defect which projects a faint shadow onto the page composer mask. Figure 9(b) shows the object beam illumination in the hololens plane, to a different scale, which is mixed with the reference wave to form the hololens hologram. During operation of the memory system, a pattern of identical geometrical shape and size is projected by the object beam lens onto the erasable storage medium to record the page composer information.

It can be seen in Fig. 9(b) that the ratio a of the nominal hologram width of 1 mm to the diameter of the central disc of the object beam pattern is 2.3, as specified in the final design of the optical system. Since the hologram size is much larger than is required to resolve the image of the page composer, the extra area can be used to provide additional redundancy. This is accomplished by imaging more than one point source onto each hologram area. Additional point source images are easily obtained by interposing crossed sinusoidal phase gratings between the multiple lens array and the page composer mask in Fig. 8. The result, shown in Figs. 10(a) and (b), is the addition of uniform structure in the image of each element of the page composer mask, and the averaging out of cosmetic defects

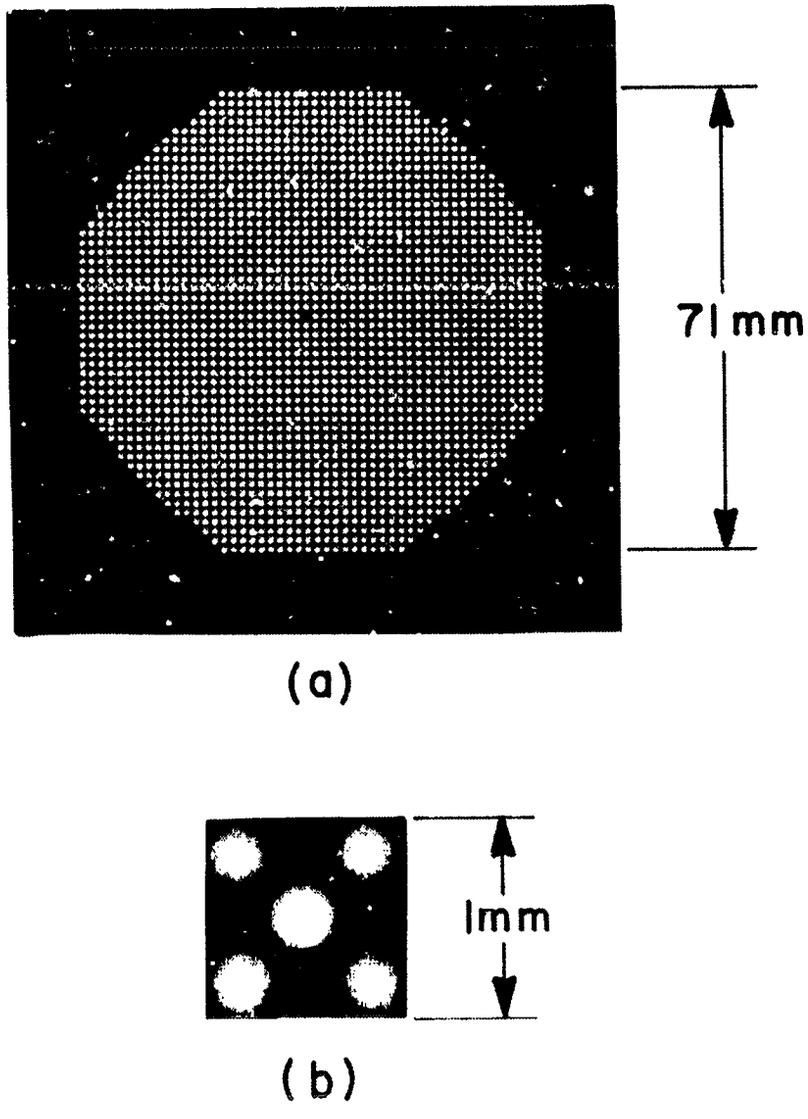

Figure 10. (a) Image of page composer mask, with redundancy added by a grating.
(b) Corresponding object illumination of one hologram in hololens array.

in the illumination from the lenslets. There remain in Fig. 10(a) some low contrast interference bands caused by overlapping higher diffraction orders from separate lenslets. This effect is easily eliminated by slightly rotating the crossed gratings in their own plane to remove the overlapping orders.

The large area available for recording each hologram on the hololens, and on the erasable storage medium, also permits the use of diffuse illumination. The scatterer of Fig. 9 can be a plate of frosted glass in this case. Figure 11 is an enlarged image of the portion of the page composer mask surrounding the central opaque element, taken through the 1-mm hologram aperture with diffuse illumination.

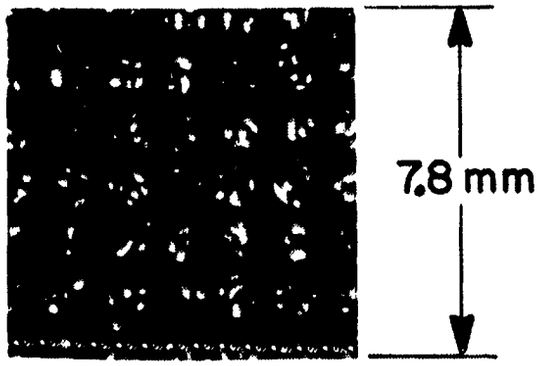

Figure 11. Image of page composer mask, diffusely illuminated, as seen through 1-mm hologram aperture.

It can be seen that there are seven or eight resolvable points in the image of each page composer element. Although there are large fluctuations in intensity among the resolvable points, the light flux averaged over each page composer element is much more uniform. When the ratio a approaches unity, the number of resolvable points for each page composer element also approaches unity. The image intensity fluctuations would then be so severe as to rule out the use of diffuse illumination.

The dichromated gelatin holograms were prepared from commercial photographic plates (Kodak 649-F and High Resolution Plates) by first removing the light-sensitive silver salts to leave a layer of gelatin on glass, then sensitizing the gelatin in a dichromate solution, followed by development in water and alcohol after the holographic exposure. The precise steps, which are similar to those widely described in the literature, are listed below.

Preparation:

(1) Agitate for 5 minutes in Kodak Rapid Fixer with hardener, mixed as directed.

(2) Rinse in flowing water for 10 minutes.

(3) Dip briefly in 1:200 solution of Kodak Photoflo 200 and water.

(4) Hang vertically to dry at least 24 hours.

Sensitization:

(1) Agitate for 5 minutes in solution of 100 grams of ammonium dichromate in 1 liter of water. Mix fresh solution every 5 days.

(2) Dip briefly in 1:200 solution of Photoflo 200 and water.

(3) Hang vertically to dry in darkened room for 2 hours.

(4) Remove dehydrated crystallites of dichromate from back of glass plate with damp towel. Paint back with fast-drying flat black paint to suppress reflections. Use red or yellow safelight.

(5) Expose plates within approximately 12 hours.

Development:

(1) Develop for 5 minutes in solution of 5 grams of ammonium dichromate in 1 liter of water.

(2) Place in standard solution of Kodak Rapid Fixer with hardener for 5 minutes.

(3) Rinse in flowing water for 5 minutes. Then, place the holograms for

(4) 1 minute in 1:200 solution of Photoflo 200,

(5) 2 minutes in 50% isopropanol well mixed with water,

(6) 2 minutes in 75% isopropanol and water solution,

(7) 2 minutes in 90% isopropanol/water solution, and

(8) 2 minutes in 100% isopropanol bath, covered with plastic bag with dry nitrogen inlet.

(9) Hang the plate vertically to dry above bath in dry nitrogen for 30 to 60 minutes.

Filtered tap water is used, and all baths are maintained at room temperature. Typical exposures of 100 mJ/cm^2, with a reference/object intensity ratio of 20:1, required 5 minutes to record over the 7-cm-diameter hololens area. Reproducibility is only fair in these circumstances. Hololens arrays were obtained in which the zero and first order outputs were 65% and 8%, respectively, of the incident beam intensity when aligned at the appropriate playout angle. This gives a hololens with an 8:1 beam splitting ratio and an optical system efficiency of 73%. The remaining light is lost by surface reflections, scattering, and absorption. A sealed cover glass plate over the gelatin is necessary to prevent gradual loss of diffraction efficiency in environments of high relative humidity ($\geq$ 70%).

B. Object and Readout Lenses

Two compound imaging lenses are required for the holographic memory system. The object beam lens images the hololens array onto the storage medium. The page composer is placed as close as possible to this lens and serves as the effective aperture stop of the lens. The readout lens projects the virtual image of the page composer, as reconstructed by wavefronts from the erasable holograms, onto the photodetector array. The storage medium is located as close as possible to this lens and also forms the effective aperature stop. Both lenses are required by the memory system design to operate at unity magnification with identical focal lengths. Although a somewhat smaller aperture is required for the readout lens than for the object beam lens in the final design, identical design specifications were chosen.

Specifications that were chosen for the imaging lenses are listed below with a brief discussion where necessary. The first six items follow directly from the final design specifications for the memory system given in Section II of this report. The last two items are tolerances on image quality.

(1) Wavelength — 488.0 nm, monochromatic.

(2) Magnification — 1:1.

(3) Focal length — nominally 175 mm. Axial distance between image plane and aperture stop is 356 mm.

(4) Object diameter — 71 mm.

(5) Image diameter — 71 mm.

(6) External aperture stop —

(a) Diameter — 71 mm.

(b) Location — At least 6 mm outside the end of the lens barrel on the image side. It is required that this aperture be fully and uniformly illuminated by any point in the object plane.

This specification guarantees that the page composer can be fully illuminated by every hologram in the hololens array. Also, all readout image rays will reach the photodetector array from every hologram in the erasable storage medium.

(7) Resolution — the image blur from any object point will be less than 0.2 mm in diameter. This specification for the object beam lens requires that all rays which would ideally arrive at one point on the storage medium must arrive within one-half the diameter of the main lobe of the diffraction pattern from one page composer element. This ensures that a substantial fraction of the light from all page composer elements illuminates the hologram area, rather than spreading over a larger area. For the readout lens, the specification requires that the image shift from hologram to hologram be less than one-fourth the diameter of one page composer element.

(8) Distortion — for any object point, the center of the image circle will deviate no more than 0.3 mm from the corresponding undistorted image point. For the object beam lens, this specification ensures reasonably accurate overlap between the object beam and the reference beam for writing holograms anywhere on the erasable storage medium. For the readout lens, distortion shift of the image is less than one-third the diameter of a page composer element.

The aberrations of two-element cemented lenses are too severe to fulfill these requirements. A commercially available 8-element 174-mm, f/1.4 flying spot scanner lens gives adequate image quality, but cannot provide illumination of the entire external aperture as required. The lenses used in the system were custom designed and fabricated by Tropel, Inc. The barrel is 120 mm in diameter by 167 mm long; it contains six elements having an effective focal length of 230 mm, giving f/3.1 at infinity. Image blur diameter is less than 0.06 mm and distortion is less than 0.025 mm.

V. LIQUID CRYSTAL PAGE COMPOSER

The transmissive liquid crystal page composer (LCPC) used in this system contains 2,048 circular elements arranged in a quasi-octagonal pattern. The elements are 0.976 mm in diameter and are spaced on 1.30-mm centers. The bits are push-pull in nature with one pair of elements representing a single bit for reasons that are detailed in the description of the detection system. The two elements of a bit operate in complementary fashion with one element energized with an ac voltage and the other unenergized. With no voltage across it, the nematic liquid crystal is transparent and light is transmitted unimpeded. A voltage across the liquid crystal material causes it to become turbulent so that light passing through it is scattered strongly with little light reaching the selected storing page to be recorded. In the differential mode of operation, the "1" and "0" are determined by which one of the two elements of a bit is energized.

The LCPC is partially controlled in the sense that only 10 of the bits are electrically alterable while 1014 bits are fixed bits with half the elements scattering and the other half clear in an unchanging pattern. The page composer is fully populated, however, because it contains 2,048 elements of which 1,024 bright spots always get recorded in and played out from a hologram. The 10 alterable bits have been located around the periphery of the pattern and at its center so that results are representative for bits located anywhere in the LCPC. Nearest neighboring bits have also been included so that interaction effects between bits could be studied.

A cross-sectional view of the LCPC is shown in Fig. 12. Two glass plates with transparent electrically conductive coatings sandwich the nematic liquid crystal material between them at a separation of 0.0127 mm as determined by Mylar spacers. The conductive coating on glass 2 is etched to form the pattern shown in Fig. 13 to which voltage can be applied to energize half of the fixed elements and the 10 selected alterable elements. The pads for wire connections to the drive electronics are also visible. The transparent conductive layer on glass 1 is not etched but is left intact to serve as a ground plane or counterelectrode for the electrodes of glass 2. In addition, an opaque layer of aluminum is deposited on the transparent conductive layer of glass 1 to form the pattern shown in Fig. 14 which defines all of the 2,048 elements of the LCPC by masking the regions between the outside of the circular elements. This pattern is then registered precisely with the pattern of Fig. 13 on glass 2 when the sandwich is put together. The task of aligning the LCPC in the optical memory system is significantly eased and simplified because of this built-in mask.

A page composer was assembled with plates as described above and was hermetically sealed and mounted on a holder with micrometer position controls. When the LCPC was electronically activated and tested in a simulated optical memory system using helium-neon laser light, contrast of better than 50:1 was measured at a detector for the clear state vs. the scattering state of a liquid crystal element. Birefringent effects in the liquid crystal material were also measured and were found to reduce the usable light at the corners of the LCPC by about 25%. After these tests, the LCPC was

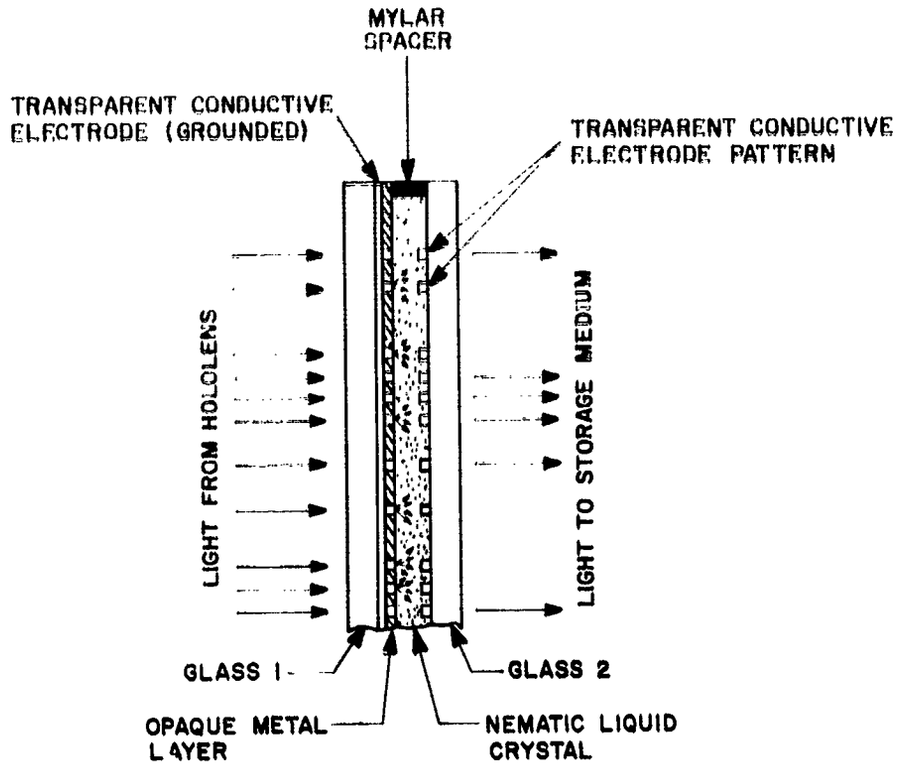

Figure 12. A cross-sectional view of the liquid crystal page composer.

incorporated into the read-write optical memory system and has operated successfully with all the other components of the system. See Fig. 15.

The lifetime of a liquid crystal cell is strongly dependent on the method used to seal it which determines the contamination level in the cell. One cell, which was filled first and then sealed with a silicone rubber epoxy, started showing signs of deterioration after about one month. We suspect that uncured epoxy in direct contact with the liquid crystal material was responsible. Degradation occurs in the form of apparent misalignment of material such that scattering centers producing a frosted or cloudy appearance can be seen at some locations with the material in its clear unenergized state. This, in turn, decreases the obtainable contrast ratio. A better fabrication technique was developed in which the seal with the epoxy was made first except for one small port for entry of the liquid crystal and one for exit. The cell was then filled after allowing time for the epoxy to cure to a more inert state. A cell made this way operated well for one year before some tiny spots of contamination appeared. There are other difficulties associated with the fabrication of large-area cells such as entrapped air bubbles, misaligned regions of nematic material, surface contamination in the sandwiching plates, short-circuits between electrodes and the ground plane, etc. RCA at Somerville, N.J., has developed techniques for making large cells -- some as big as 20 cm × 20 cm -- involving a glass frit seal and a controlled pressure-vacuum filling station. Cells made there have operated for several years with no contamination difficulties. However, the specific production conditions must be tailored to the particular cell involved so that numerous trial runs might be necessary to establish the

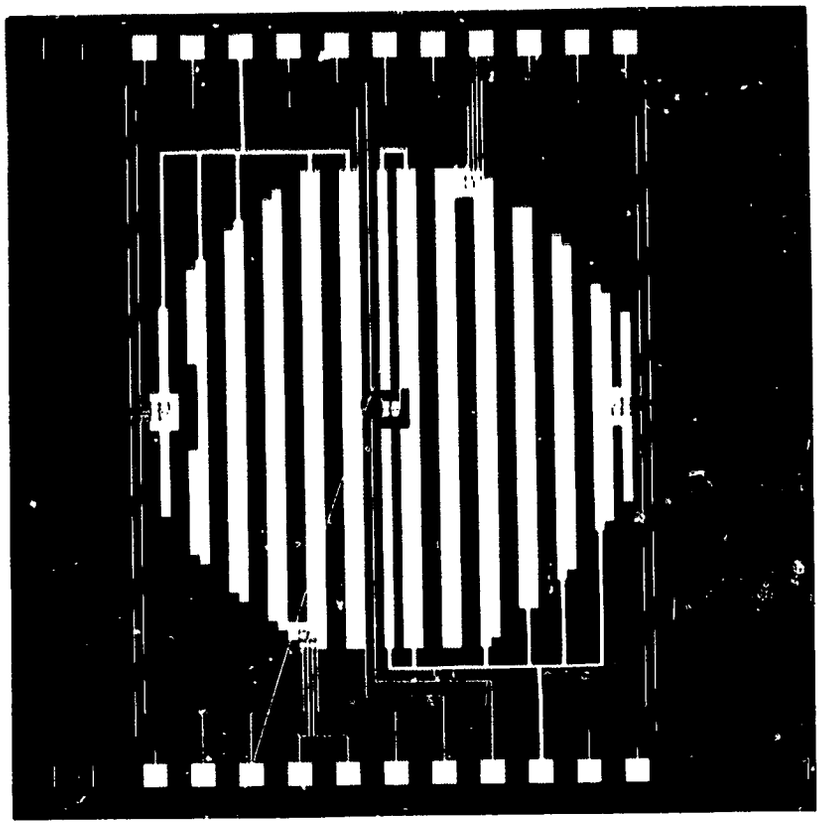

Figure 13. The transparent conductive electrode pattern on glass 2.

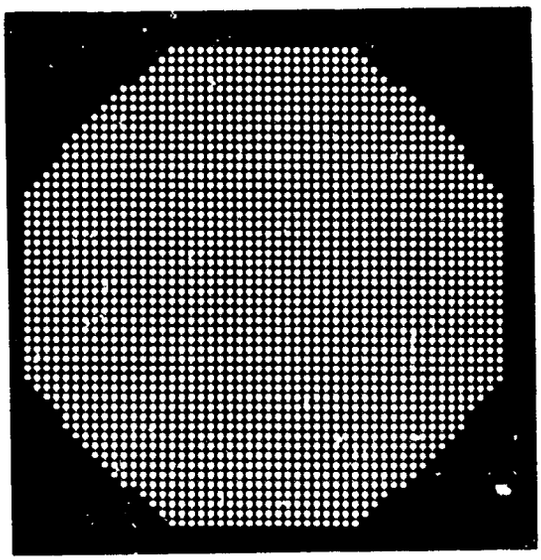

Figure 14. The opaque aluminum pattern formed on glass 1.

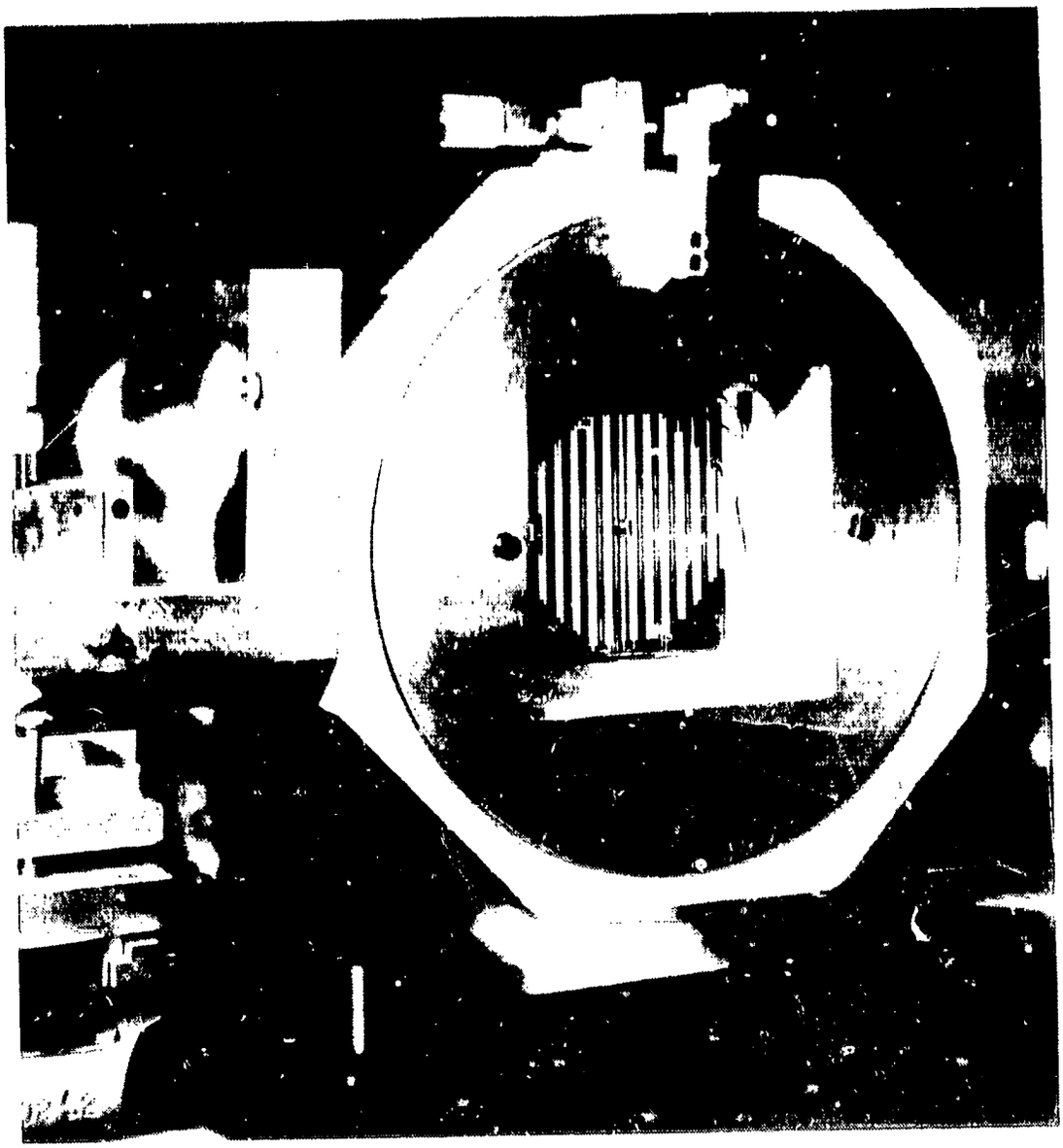

Figure 15. The 1024-bit liquid crystal page composer mounted on its holder and activated to produce a typical pattern of scattering.

proper values for all of the system variables. Since we needed only a few cells, we felt that it would be more expeditious to work with the group doing research on liquid crystals at RCA Laboratories, even though the available facilities and experience with large cells were not equivalent to those at Somerville.

VI. ERASABLE STORAGE MEDIUM

The requirements for the storage plane in the prototype read-write holographic memory were:

Resolution in excess of 1400 lines/mm

Sensitivity to 4880 Å (~ 490 nm) radiation

Transmissive readout

Total size greater than 7.6 cm

Page size 1 mm

Write energy ~ 1 mJ or less

Read efficiency ~ 1% or greater

To satisfy these requirements it was decided that a thermoplastic-photoconductor sandwich would be used for the storage plane. The thermoplastic material used was Staybelite ester 10 (Hercules Powder Corp., Wilmington, Delaware) and the photoconductor used was poly-n-vinyl carbazole doped with 2,4,7 trinitro fleurenone (Polysciences Corp., Warrington, Pennsylvania).

In the following, we will describe material preparation, storage plane fabrication, and the operating parameters of the storage plane. Some interesting techniques that allow operation on a large storage plane will also be covered.

A. Materials

1. Photoconductor. — The photoconductor used in all experiments was poly-n-vinyl carbazole (PVK) doped with 2,4,7 trinitro 9-fleurenone (TNF). These were mixed in the ratio 5 gm of PVK to 1 gm TNF and then diluted in 100 ml of 1,1,2 trichlorethane. In early experiments the solvent used was an equal mixture of p-dioxane and dichloromethane, but this had the disadvantage of too rapid evaporation of the solvent which led to problems of repeatability and to problems of film formation in humid atmospheres. The sensitivity of this photoconductor will be discussed later.

2. Thermoplastic. — The thermoplastic used in most of the experiments was Staybelite ester 10, a derivative of a natural tree resin. Various solvents were used, but the preferred solvent was hexane. The Staybelite ester 10 was diluted in the hexane in the ratio 20 gm of Staybelite to 100 ml hexane.

3. Substrate. — The substrate used was InO-coated glass (Nesatron, Pittsburgh Plate Glass Co.), with electrical conductivity in the range 50 to 100 ohms per square. The InO coating was etched into the desired pattern using a dilute hydrochloric solution. The active areas of the partially populated storage medium were 1 mm^2 squares distributed as shown in Fig. 16. The total pattern of the substrate, including evaporated gold lines used to bring power to the active areas, is shown in Fig. 17.

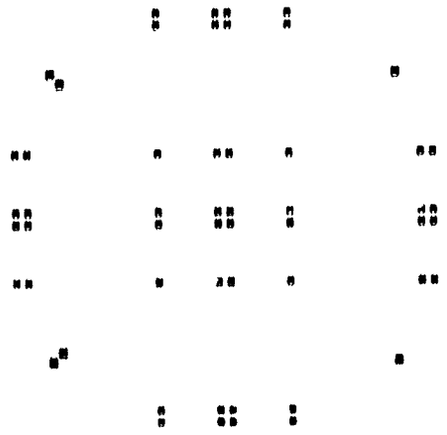

Figure 16. Active storage locations, shown actual size.

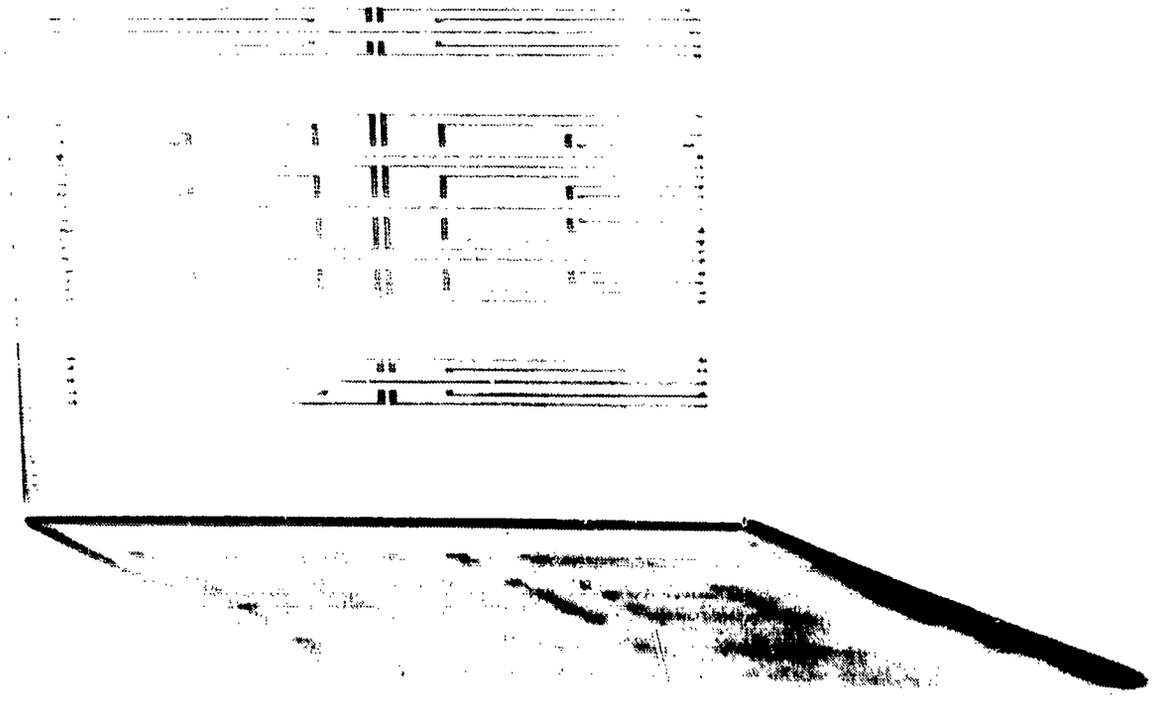

Figure 17. Complete storage plane, showing gold lines to activate areas.

B. Sample Fabrication

The technique used for sample fabrication was dip-coating, with the photoconductive layer applied first and the thermoplastic layer applied next.

The technique of dip-coating involves the careful withdrawal of a substrate from a solution of the material to be coated. To obtain smooth films, care must be taken to avoid changes in withdrawal speed and to avoid mechanical vibrations. The thickness of the deposited film can be controlled either by varying the speed of withdrawal or by changing the viscosity of the solution; in most experiments the first method was used.

The apparatus used is shown in Fig. 18. To achieve constant speed a synchronous motor was used, and a large flywheel was put on the drive shaft. To avoid slippage a toothed belt and pulley were used. To avoid disturbance caused by air motion a tall tank was used to hold the solution.

The speed of withdrawal, and hence the thickness of the deposited layer, was varied by the use of different-diameter pulleys. The uniformity of the deposited film was fair; variations in thickness of the order of several hundred angstroms were observed.

As mentioned above, the photoconductor was deposited first. The plate was allowed to dry for several minutes and was then submerged in the thermoplastic solution. (If necessary, the pulley was changed while the plate was drying.) After the thermoplastic layer was deposited the plate was placed in an oven at 60°C for one hour.

C. Recording on Thermoplastic Media

The basic principles of storage have been discussed in the literature (refs. 1—3), and in Volume II of this report. The operation involves the sequential processes of charging, exposing, recharging, and heating. Erasure is accomplished by reheating the film.

To ensure repeatable results and to avoid catastrophic electrical breakdown of the thin thermoplastic film, the voltage on the film (due to the corona charging) must be precisely controlled. This control is complicated by the need for random selection of storage locations over a large storage plane for a number of reasons. The fact is that it is hard to uniformly corona-charge an area as large as that shown in Fig. 16 (7.5 cm × 7.5 cm). The second reason is that because of random selection, one location may be repeatedly selected (and therefore charged and heated) but another location on the same plane may be only charged. If not controlled, the voltage on the unselected location will rise to the breakdown voltage of the film and cause damage. A third reason is that corona-charging is affected by atmospheric conditions such as humidity and temperature. The variation in these conditions normally encountered will lead to changes in the voltage on the thermoplastic.

The first of these problems, corona-charging a large area, was solved by using the corona applicators shown in Fig. 19. It consists of fine (50 to 75 μm diameter) wires held in a "serpentine" pattern by a plastic frame over the storage plane. The distance from the wires to the plane, and between each

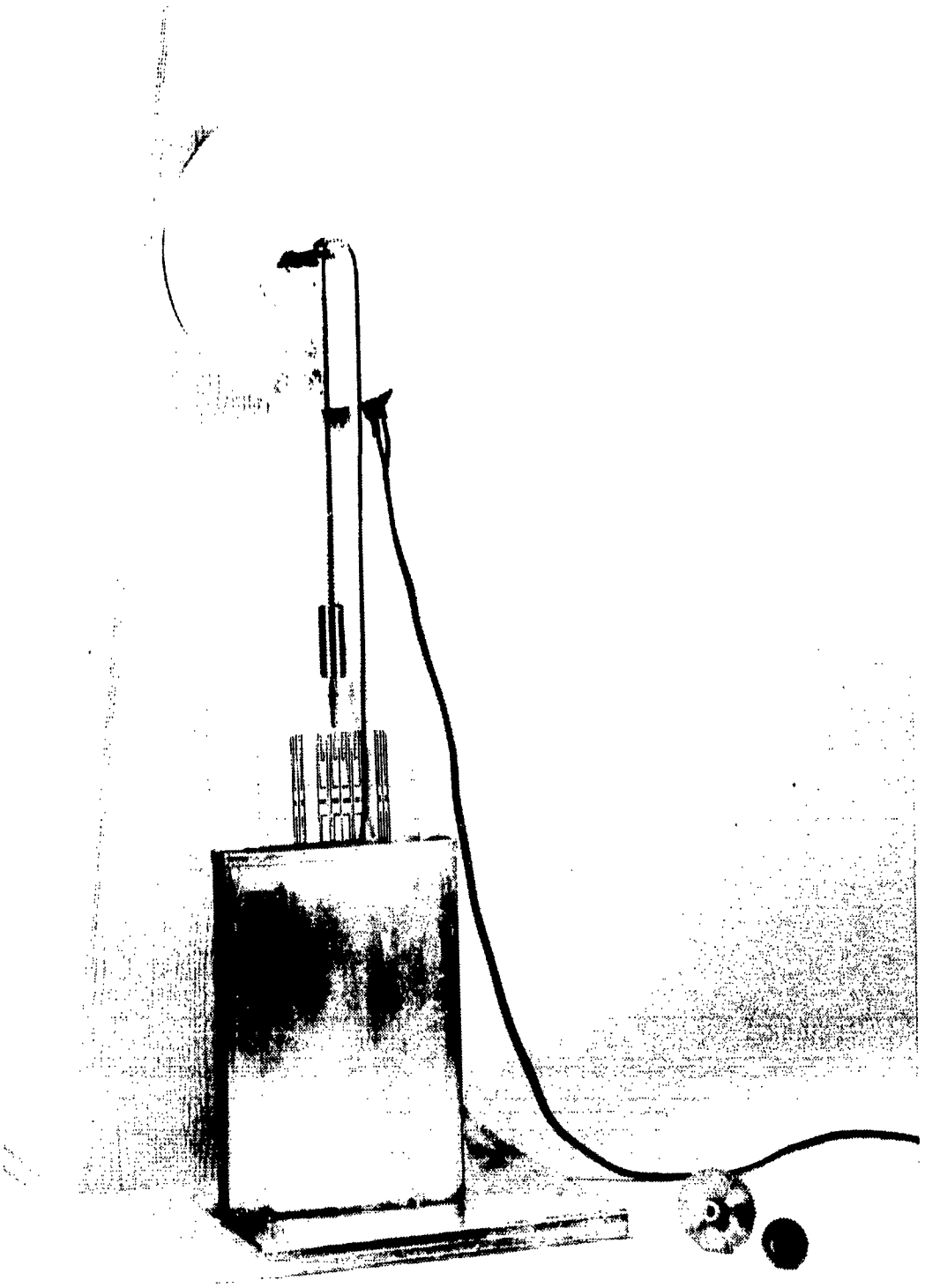

Figure 18. Apparatus for dip coating.

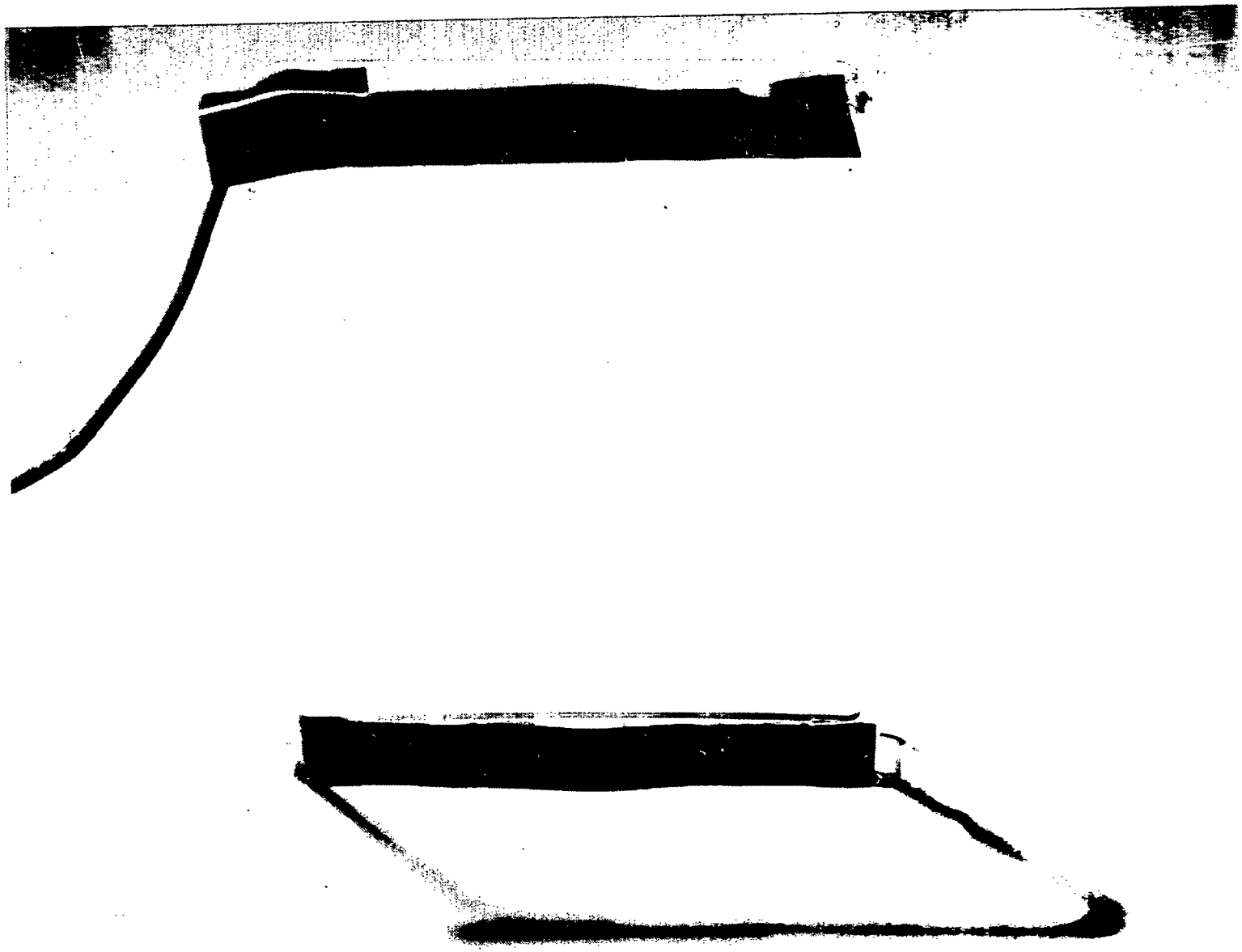

Figure 19. Corona applicator.

wire, is approximately 1 cm. The wires are fine enough, and far enough away from the storage plane, so they do not intercept an appreciable part of the light.

This arrangement does charge the entire storage plane. It is not uniform, however, since the edge or external wires emit more charge than the inner wires. (The cause can be attributed to wire-to-wire capacitance effects.)

To solve the problem of nonuniform charging, and the more important problem of precise voltage control, a grid (apertured metal plate) was placed over the storage plane. The grid used for the prototype system, with apertures at the active locations of the storage medium, is shown in Fig. 20. For a fully populated storage plane the grid would take the form of a mesh. In use, the apertured plate is placed against the storage plane | separated only by a thin insulating film (25 μm thick) to prevent short-circuits |, and voltage, equal to the desired voltage on the thermoplastic film, is applied to it. This prevents the voltage on the thermoplastic caused by corona-charging from rising above the voltage on the apertured plate. The reason is that if the voltage at the thermoplastic were to rise above the grid voltage, the ions of the corona carrying the charge would be deflected to the grid. We found that, with the use of the grid, the maximum voltage on the thermoplastic was substantially independent of charging time and of voltage on the corona applicator. The use of the grid allowed highly repeatable results. The complete system, with all elements in place, is shown in Fig. 21.

Two of the more important characteristics of the thermoplastic storage media are its sensitivity (that is, efficiency as a function of exposure) and its spatial frequency characteristics (that is, efficiency as a function of the angle between object and reference beams).

Figure 22 is a typical plot of the efficiency of the reconstruction as a function of the exposure. In this particular experiment the photoconductor thickness was 1.5 μm, the thermoplastic thickness was 0.5 μm, and the grid voltage was 200 V. The beam ratio used in this experiment was 1:1.

Besides the gratifying result that the thermoplastic medium is quite sensitive (of the order of 649F photographic film), there is the interesting result that the efficiency remains constant even for relatively high exposures. Further study of this aspect of thermoplastic recording shows that this feature is a consequence of using a 1:1 beam ratio in the experiment.

The reconstruction efficiency is not a monotonic function of the recording esposure. In the following analysis we derive the variation of efficiency versus exposure. We use a lumped-circuit model, consisting of a capacitor shunted by a resistor, to describe the photoconductor, and we make the assumption that the effect of light on the photoconductor is to vary the value of the shunt resistor. Although this model is admittedly somewhat naive, its virtue is that it predicts the experimental results quite accurately.

In this analysis we confine our attention to the voltage across the photoconductor; this voltage determines the ultimate forces acting on the thermoplastic.

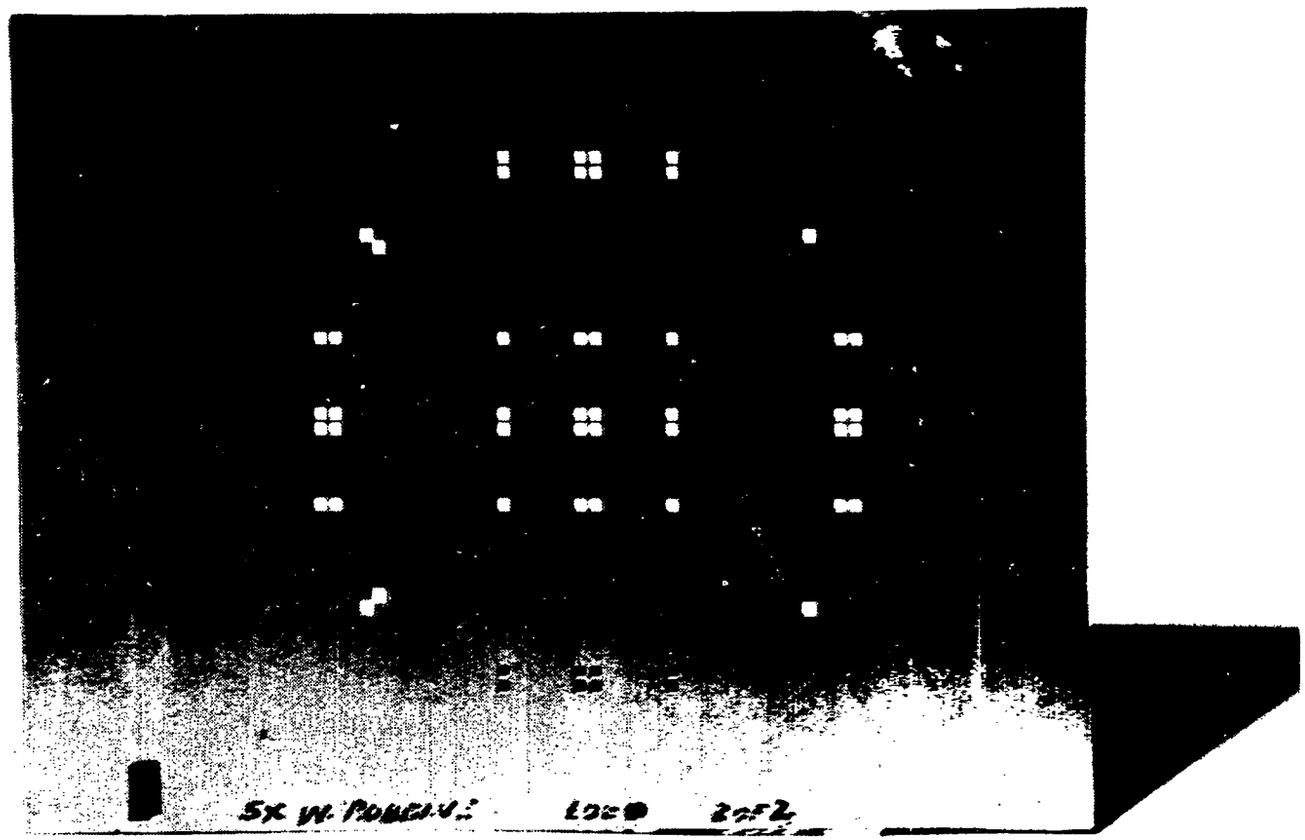

Figure 20. Metal grid used for voltage control of thermoplastic surface.

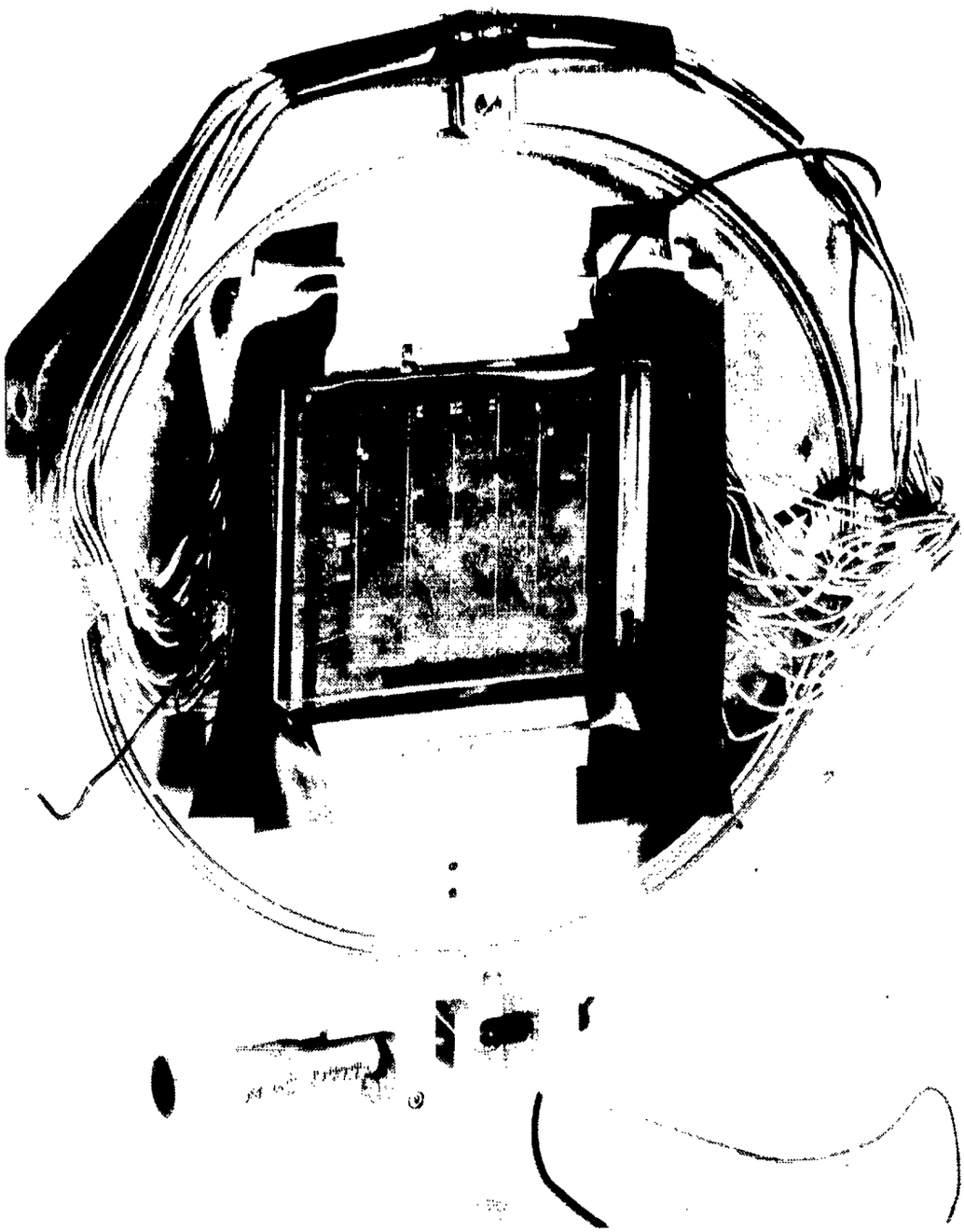

Figure 21. Storage plane, assembled and mounted.

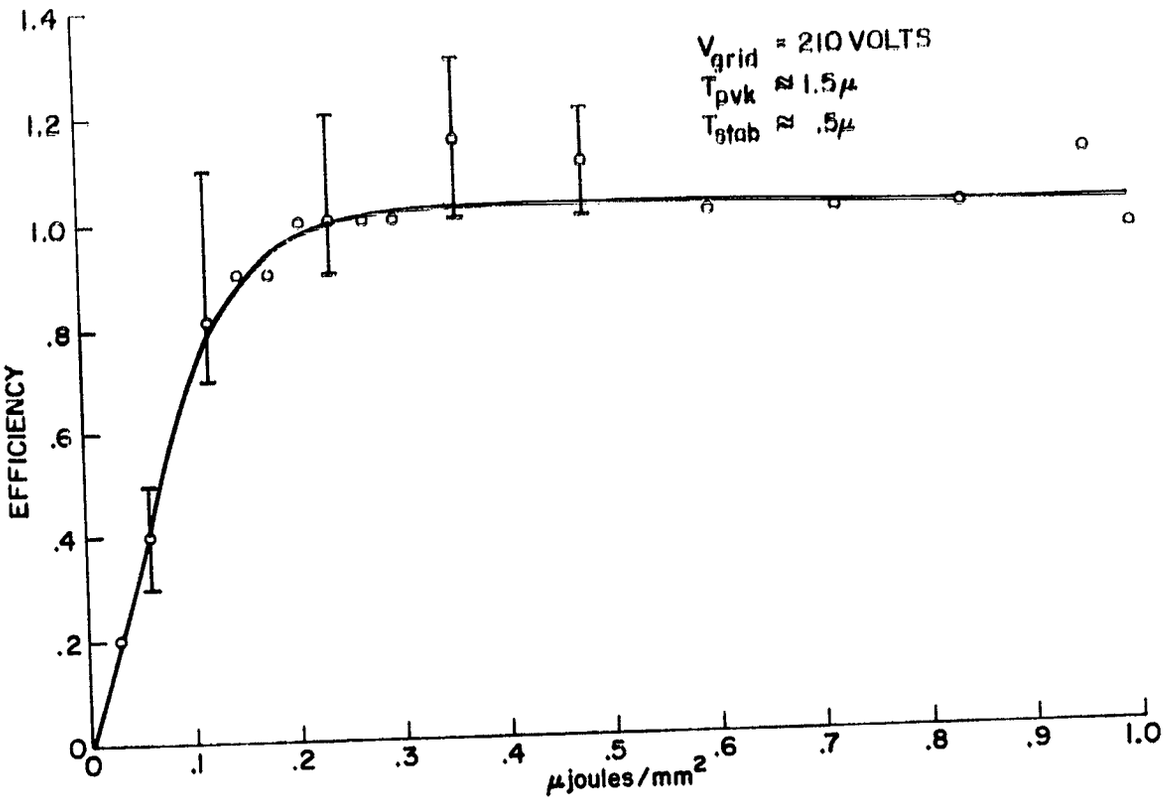

Figure 22. Measured hologram efficiency versus exposure; unity beam ratio.

Using the lumped-circuit model, the relationship for the voltage across the photoconductor is

$$C\frac{dV}{dt} + GV = 0 \tag{30}$$

where C is the capacitance per unit area and G is the conductance per unit area. If we assume that the conductivity of the photoconductor varies with the intensity of the absorbed light and we further assume that the intensity is written as

$$I = I_o\left(1 + m\cos\frac{2\pi x}{d}\right) \tag{31}$$

we have

$$C\frac{dV}{dt} + KI_o\left(1 + m\cos\frac{2\pi x}{d}\right)V = 0 \tag{32}$$

where K is a proportionality factor (the sensitivity of the photoconductor), m is the modulation ratio, d is the spatial wavelength, and x is a dimension on the surface of the photoconductor. The solution to this equation is

$$V(x,t) = V_o \exp\left[-KI_o\left(1 + m\cos\frac{2\pi x}{d}\right)t\right] \tag{33}$$

The thermoplastic behaves like an incompressible fluid, which implies that its motion is not dependent on the absolute forces applied, but rather on the spatial variation, or difference, of the applied force. From the previous relationship we note that the maximum voltage (related to the maximum force) is

$$V = V_o \exp[-KI_o(1 + m)t] \tag{34}$$

and the minimum voltage is

$$V = V_o \exp[-KI_o(1 - m)t] \tag{35}$$

The difference is

$$\Delta V = V_o e^{-KI_o t} \sinh KI_o m t \tag{36}$$

If we now let $I_o t$ be the total exposure E_o, we may write

$$\Delta V = V_o e^{-KE_o} \sinh KE_o \tag{37}$$

In Figure 23 we plot ΔV versus E_o, with beam ratio as a parameter. Since the ultimate behavior of the thermoplastic is dependent on ΔV, it is evident that the efficiency of the reconstructed image will not be a monotonic function of the exposure.

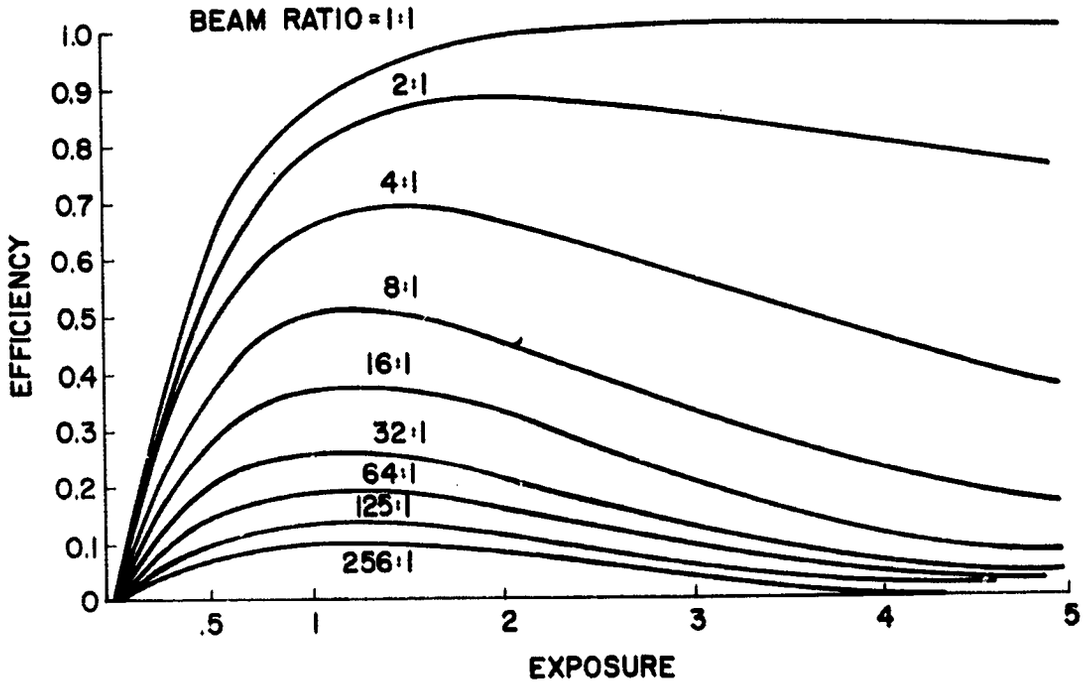

Figure 23. Calculated relative hologram efficiency as a function of beam ratio.

In the prototype system beam ratios of the order of 10:1 were used. A plot of the efficiency versus exposure for a hologram made with a 10:1 beam ratio is shown in Fig. 24.

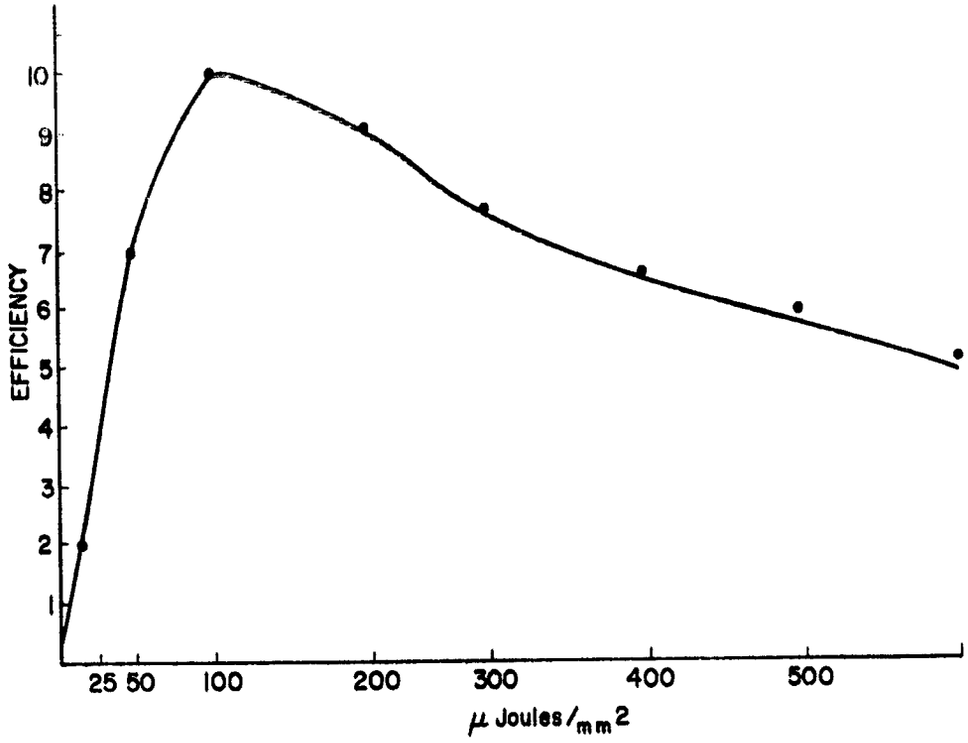

Figure 24. Measured hologram efficiency at 10:1 beam ratio.

One of the most troublesome features of thermoplastic storage is the bandpass nature of the spatial frequency response. The maximum response is centered at a spatial frequency given by 1/2h, where h is the thermoplastic thickness, and the response falls off rather quickly toward high and low spatial frequencies. Figure 25 shows, in the narrow region about the center of the band, the spatial frequency response. Figure 26 shows the response for a film 490 nm thick, which should have had a center frequency of 1000 lines/mm (corresponding to an angle of 30° between reference and object beam), while Fig. 27 shows the response for a film 340 nm thick. The dotted line in both graphs shows the angular extent of the object used in the prototype system, and we can see that the bandpass response leads to shading in the reconstruction. While this is not a disastrous result, it does lead to difficulties in readout. The more important result is that the actual center of the response curve did not occur at the spatial frequency predicted by thickness measurements made on the film.

These thickness measurements were made by interferometry, but at a location on the storage plane somewhat remote from the storage locations used for the experiment. The reasons for the discrepancy, between the predicted and actual center frequency, are either an error in thickness measurement, variations in the thermoplastic thickness over the surface of the storage plate, or a failure in the theory that predicts the center frequency. Of these, the first is the least likely, for these measurements were carefully repeated many times.

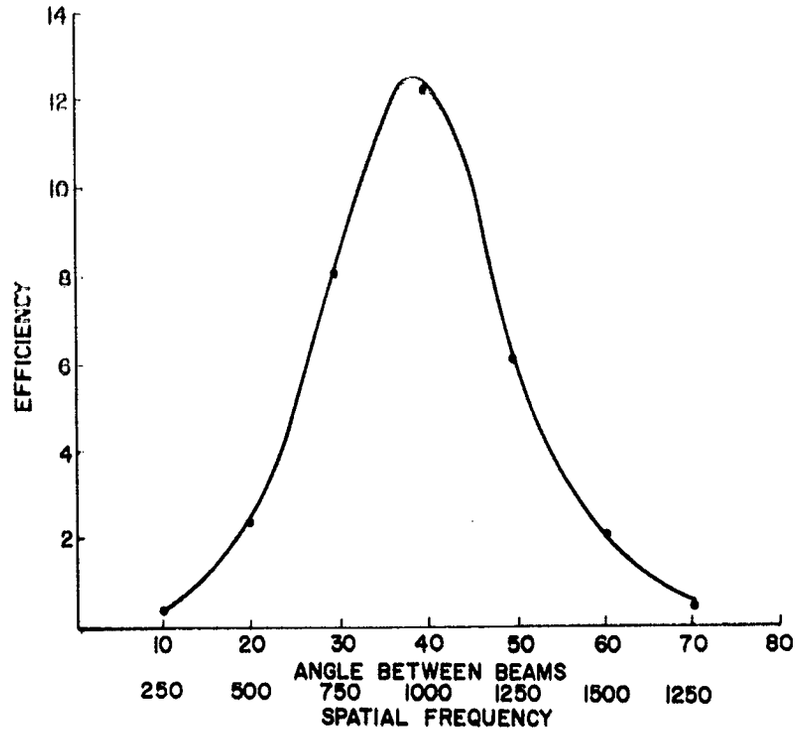

Figure 25. Hologram efficiency versus spatial frequency (from Lin and Beauchamp, ref; 2).

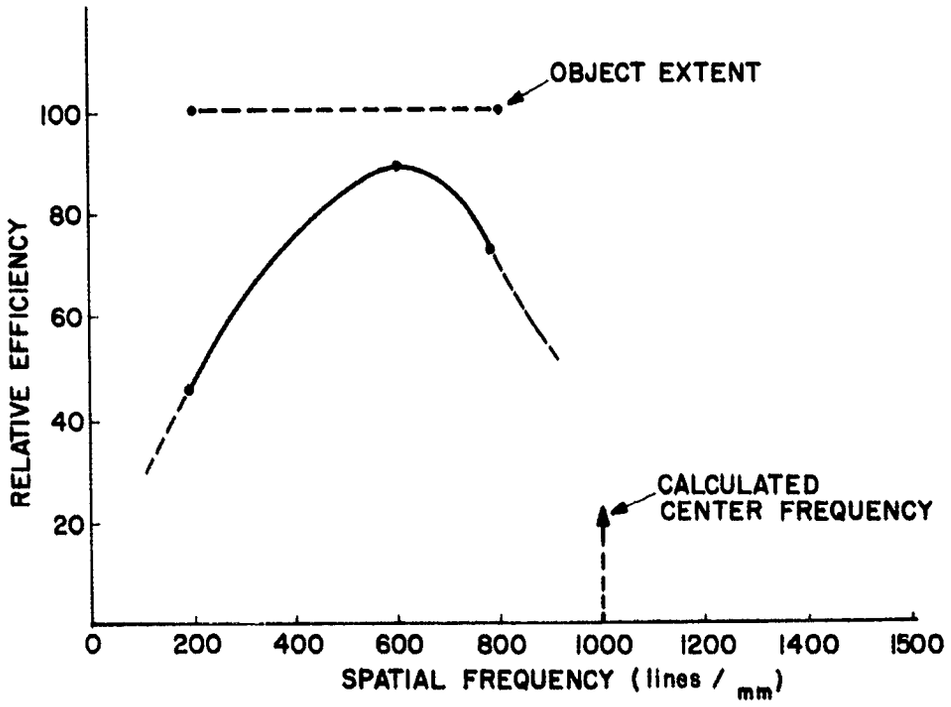

Figure 26. Hologram efficiency versus spatial frequency for a film nominally 490 nm thick.

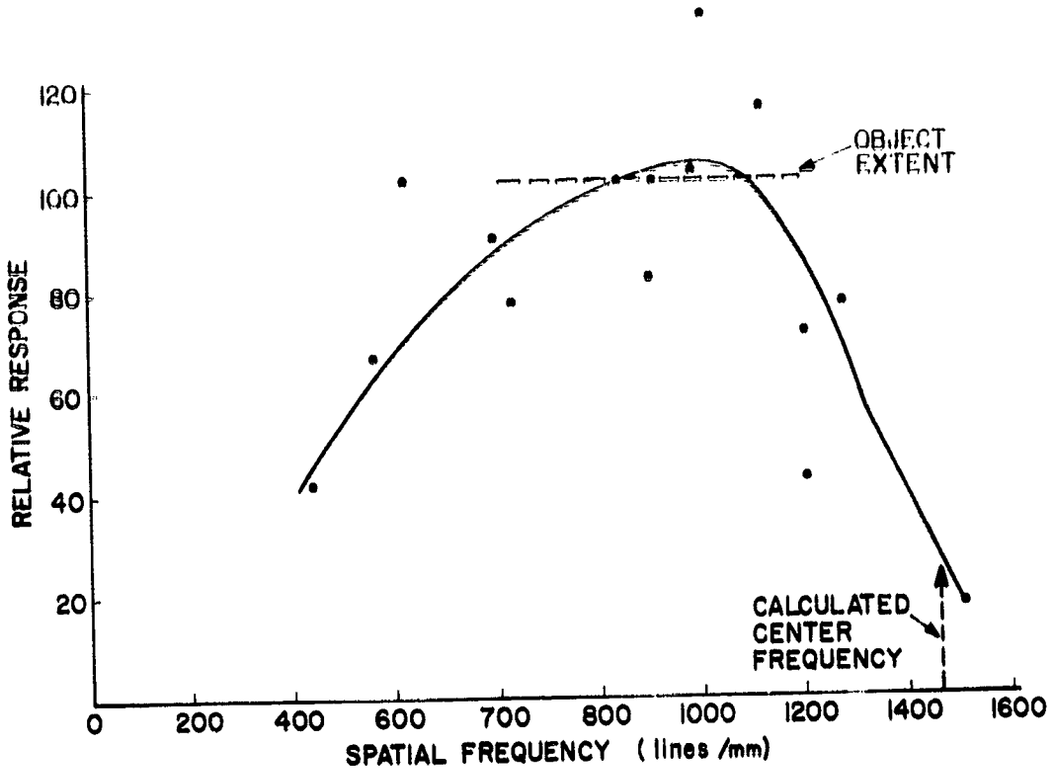

Figure 27. Hologram efficiency versus spatial frequency for a film nominally 340 nm thick.

Regardless of the cause, the results point out that it is difficult to fabricate a storage plate with predetermined performance characteristics.

An experiment was performed to find a means for thermoplastic holographic storage that would have a response independent of the exact thickness of the thermoplastic thickness. In this experiment holograms were made with the angle between object and reference beam at 45° (corresponding to 1440 lines/mm) on a storage plane with a thermoplastic thickness of 490 nm (which should result in a center frequency of about 1000 lines/mm). The thickness of the photoconductor was 1.5 μm and the voltage on the grid was 250 V. The object was the page composer used in the prototype system. The key step in the experiment was to sequentially store holograms at ever-increasing exposure and to monitor the reconstruction. That is, the complete process of erase-charge-expose-charge-read was repeated a number of times, with increasing exposures for each trial. The results of the experiment are shown in Fig. 28. The first reconstruction is expected — only the low-frequency portion of the image is visible. Then, as the exposure is increased we first see the low frequency portion of the image become brighter (all photographs made with the same exposure) and then, the first surprising result — the high-frequency portion of the image becomes visible, and a dark band separates the two positions. As the exposure is increased further the dark band is observed to sweep across the image, toward lower frequencies. Finally, at an exposure of about 800 μJ, the dark band has left the image. The effect of increasing the exposure even further appears only to brighten the image.

This experiment was repeated with storage planes of thermoplastic thicknesses that varied from 490 nm to 200 nm with substantially the same results.

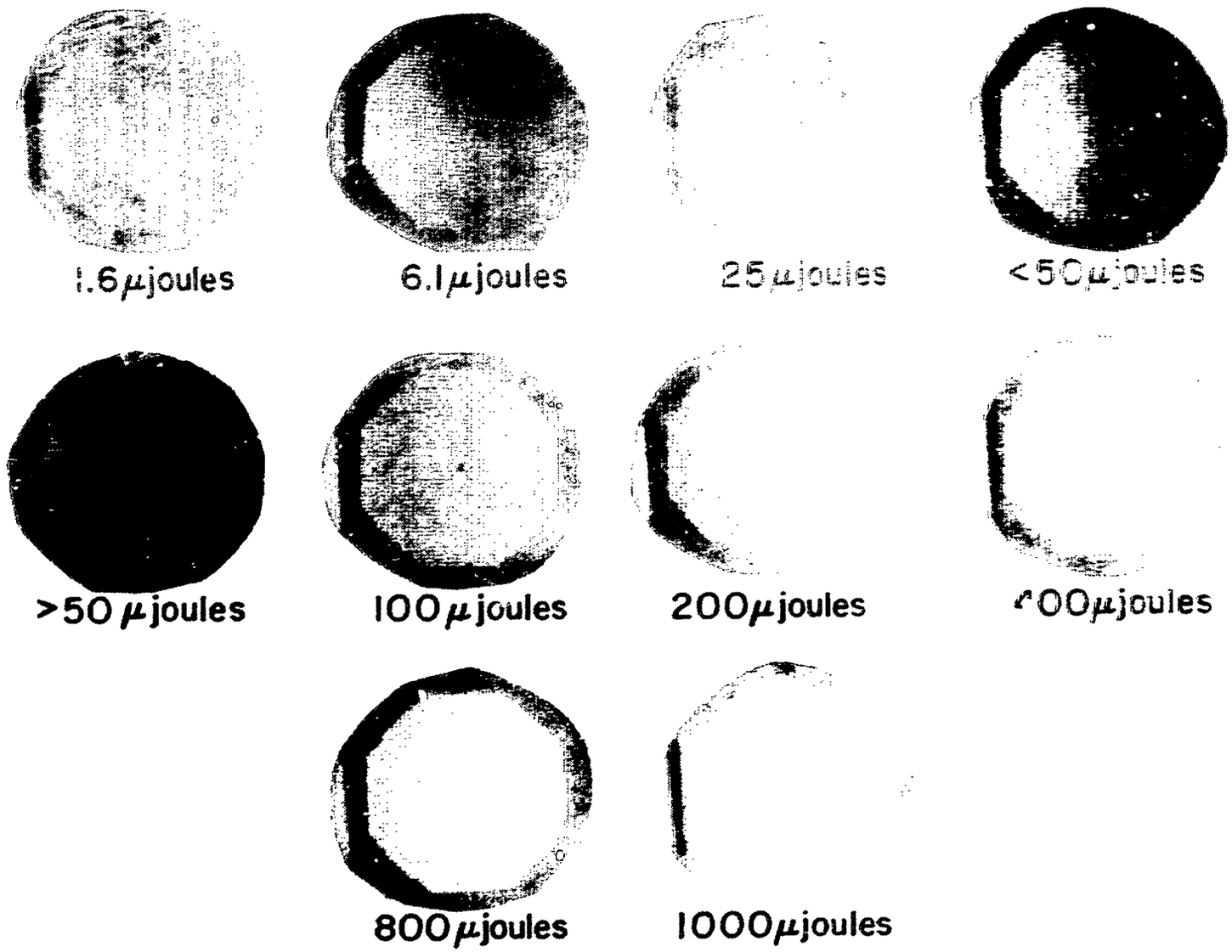

Figure 28. Spatial frequency response versus exposure, with center frequency of 1440 lines mm.

The net effect of this is that, with this approach, the exact thickness of the thermoplastic is of no consequence — a result that enormously reduces the complexity of sample fabrication. The reason for this phenomenon is not completely understood; however, it appears that at the high exposures used the photoconductor becomes saturated (or effectively perfectly conductive) while the thermoplastic itself becomes photoconductive.

The disadvantage of this technique is that it requires much higher exposures than normally used; fortunately, the prototype system had been designed for just the exposure levels needed for this method.

The final important characteristic of the thermoplastic storage medium is its fatigue behavior. While there are some thermoplastics that exhibit little or no fatigue — notably microcrystalline wax - Staybelite is not among them. The upper limit in the number of cycles that could be used before the signal-to-noise ratio of the reconstructed image became intolerable was of the order of 500. The failure was marked by the appearance of many pits and other permanent surface deformations. This was possibly caused by the lack of adequate cleanliness in the materials used, with the resulting impurities initiating the observed defects. A further cause of failure was an apparent increase in the softening temperature following prolonged operation, which was undoubtedly caused by oxidation of the thermoplastic.

Since the purpose of these experiments was the demonstration of the feasibility of holographic storage, and since it is apparent that thermoplastic materials are being developed with little or no fatigue, this aspect of the storage characteristics of Staybelite was of little practical concern.

There was one aspect, however, that was of concern. It was found that if a pattern was recorded and then retained for long periods - longer than 24 hours — it was difficult to erase. In particular, it was found that when this pattern was apparently erased and a second pattern recorded at the same location the first pattern reappeared. The first pattern was dimmer than the second, but still presented a potentially troublesome signal. It was found that this could be prevented either by not retaining a pattern for longer than 12 hours or by erasing the pattern and not using that location for at least 24 hours. Neither method is ultimately acceptable. The reason for this effect appears to be either due to cold flow in the plastic or to charge-trapping in the plastic. This is a potentially very serious problem and should be studied further if thermoplastic storage is seriously considered for holographic storage. It is not known whether this problem exists in other thermoplastic materials.

VII. PHOTODETECTOR ARRAY

An array of 20 PIN photodiodes was used to detect the ten active bits in a partially populated optical memory. Two diodes were used for each bit to indicate "1" or "0". Since both diodes feed a differential-input preamplifier, common mode light and electrical noise are attenuated.

The equivalent input noise current to each of the ten preamplifiers is about 10^{-11} A rms. This is about 6×10^{-11} W ave. of light power striking each photodiode (conversion ratio of 5A/W). While the frequency bandwidth of each tuned preamplifier is 2 kHz, the overall bandwidth of the sense system, including synchronous detection and strobing, is about 120 Hz. A redesign of the detection system could reduce the equivalent input noise current from 10^{-11} A rms to probably 2×10^{-12} A rms. At any rate, the photodetectors and the associated electronics can reliably detect an optical signal level of about 10^{-10} W ave. in about 3-msec time. However, 60 msec are required in actual operation with the optical memory because of nonuniform light levels eminating from the 20 stored spots in the storage medium and variations in gain among the amplifiers.

The ten active bits in the partially populated memory were arranged in five locations of two bits each with two photodetectors assigned to each bit. The five locations are separated about 32 mm from each other, which provides sufficient space for mounting the five clusters of four diodes each. The four PIN photodiodes of each cluster are a four-element photodiode chip. Each element is 1.3 mm square with a 0.13-mm separation. The chip is sealed in a TO-5 can with five leads extending from the base. The diameter of the light beam striking each diode is 0.97 mm, and the spacing between each of the four beams is 1.3 mm. The beam locations and diode geometry are compatible.

Alignment of the five clusters was made visually, using a jig bore machine and a microscope clamped in the drill chuck. The five clusters were easily positioned relative to one another within 0.02 mm, and each is clamped in place on the support jig, as shown in Fig. 29.

The diode array is manufactured by United Detector Technology of Santa Monica, California, and is known as PIN-Spot/4.

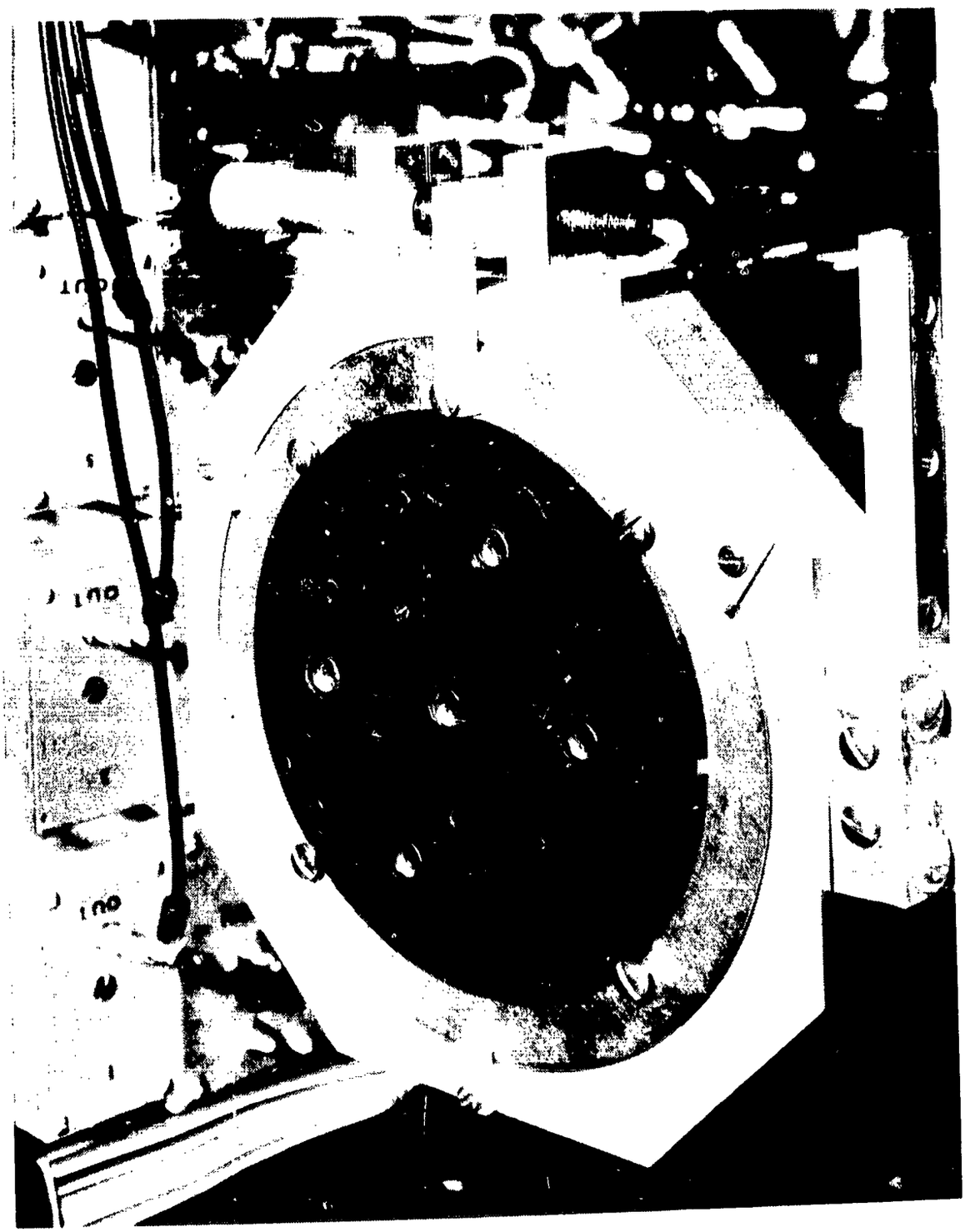

Figure 29. Assembled and mounted photodetector array.

VIII. CONTROLLER ELECTRONICS

The electronics required to operate the holographic optical memory must control five functions:

Page Composition — bits stored temporarily in page composer for later transfer to storage medium.

Page Selection — deflection of laser beam to desired location on storage medium.

Write — transfer of page composer bits to storage medium.

Read — transfer of stored bits from page to photodetectors and light display.

Erase — removal from storage medium of previously written information in any given page or pages.

An overall block diagram is shown in Fig. 30. The energizing and control units for the laser deflector, the page composer, the storage medium, and the photodetector array are each housed on separate chassis with separate front panels. Each unit can function under internal control, independently

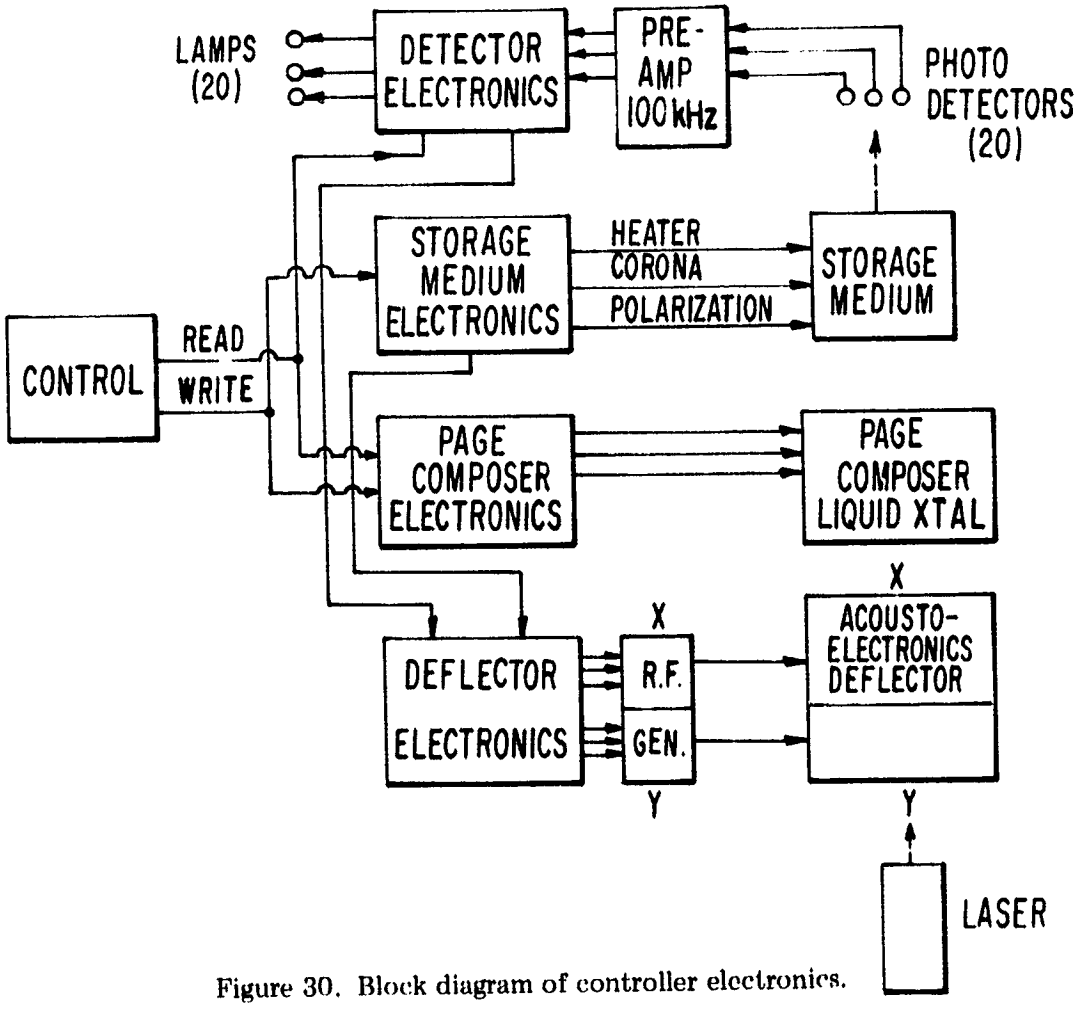

Figure 30. Block diagram of controller electronics.

of the other three, for adjustments and tests of the memory system components. For operation of the entire memory system, the four units function under external control signals from a control console, which initiates the appropriate sequence of operations.

A. Laser Deflector

This chassis provides the address logic pulses which are used by the acoustic cell drivers. The drivers generate appropriate frequencies for deflecting the laser beam to the desired page position on the storage medium. Figure 31 shows the front panel. The address pulses are 3 msec wide and occur at 30-msec intervals, resulting in a 10% duty cycle. An additional 100-kHz modulation is supplied to the y-deflector during reading as a carrier for the detector amplifiers. The number of 3-msec pulses used for reading or writing are set by front panel controls to match the sensitivity and efficiency of the storage medium. A page address is programmed by setting x- and y-positions on panel switches.

B. Page Composer

A block diagram of the page composer control electronics is shown in Fig. 32. It is composed of an array of ten pushbutton switches which drive 10 flip-flops These, in turn, control the states of the ten liquid crystal pairs of the page composer. Provisions to have all locations either clear or scattering are made. The states of the flip-flops and the liquid crystal pairs are indicated by ten pairs of lamps. A lighted bulb represents the clear element of the liquid crystal pair which would produce a spot of light on the photodetector during a subsequent read cycle. Provisions are made to electronically compose a page through the set/clear inputs of the flip-flop. The front panel is shown in Fig. 31.

The circuitry associated with the one-bit-position liquid crystal pair is shown in Fig. 33. To change a bit from the value indicated by the lamp to its complement (say from "0" to "1"), the switch is momentarily pushed. This clears and then sets a buffer flip-flop to eliminate contact bounce. The buffer then complements the data flip-flop. As previously mentioned, data can also be entered through the set/clear inputs of the data flip-flop. The data flip-flop's output is buffered to the discrete component lamp drivers and to the liquid crystal drive switches. These are mercury-wetted reed switches whose drive requirements are compatible with TTL levels and operate in several msec. The liquid crystals are driven through 100-kΩ resistors to each element. Switching is accomplished by the reed switch short-circuiting either element of a bit pair to a bus which returns to oscillator common.

The liquid crystal elements are energized by the Wien bridge oscillator/amplifier circuit shown in Fig. 34. Degenerative feedback is produced at all frequencies except that for which the bridge is balanced. The bridge balance and frequency of operation are determined by the ganged pot. The three light bulbs act to stabilize the output amplitude. The oscillator is followed by a power amplifier composed of an operational amplifier with a discrete component output stage driving step-up transformers. Feedback from the primary serves to establish the amplitude and preserve the waveshape. Amplitude control is obtained by changing the feedback. The oscillator/amplifier produces a sinusoidal waveform

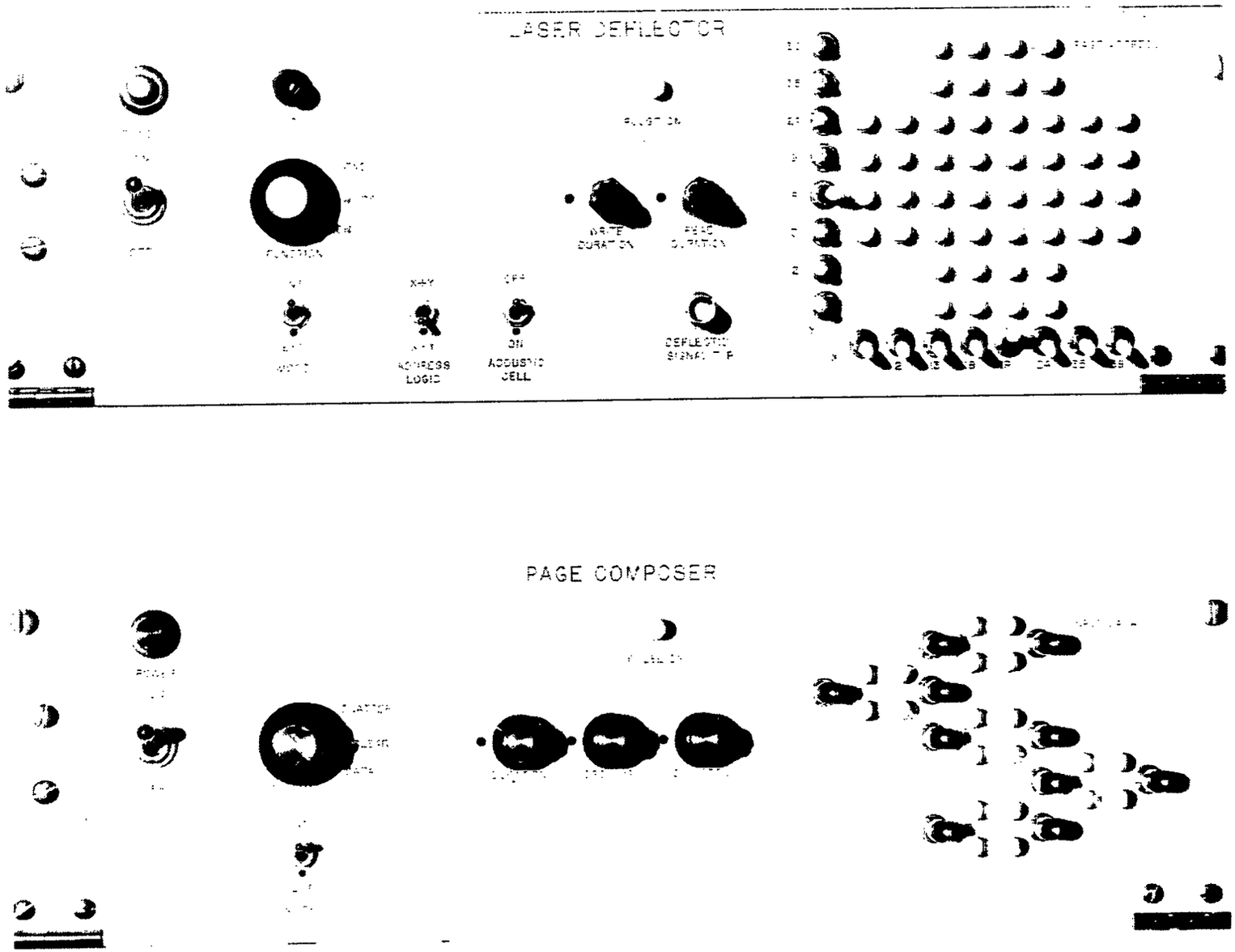

Figure 31. Front panels of the laser deflector and page composer control units.

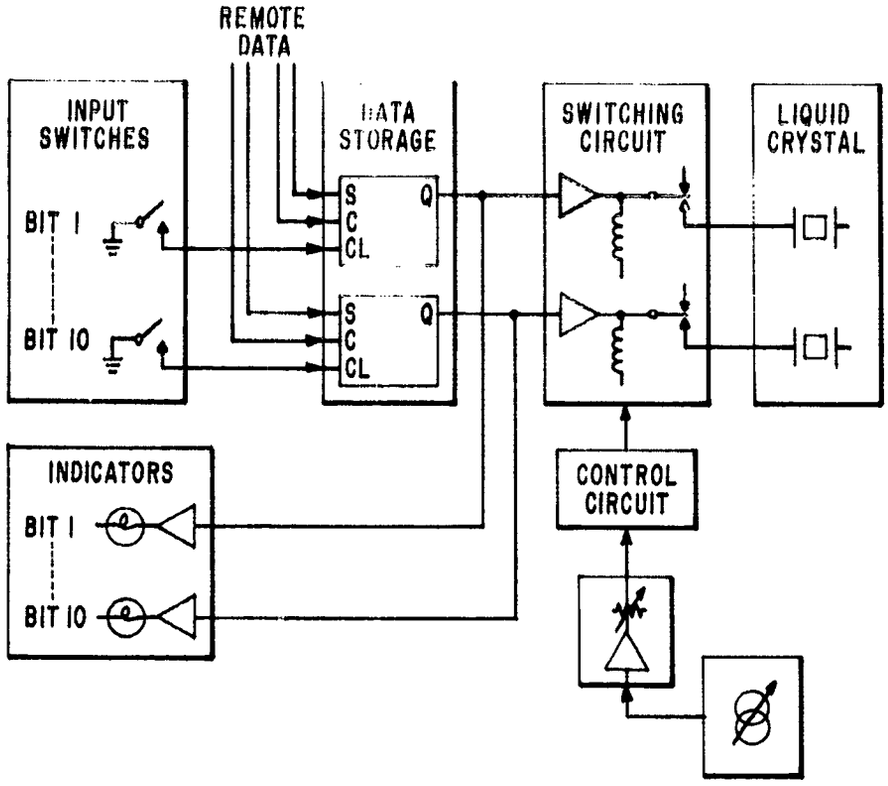

Figure 32. Block diagram of page composer control unit.

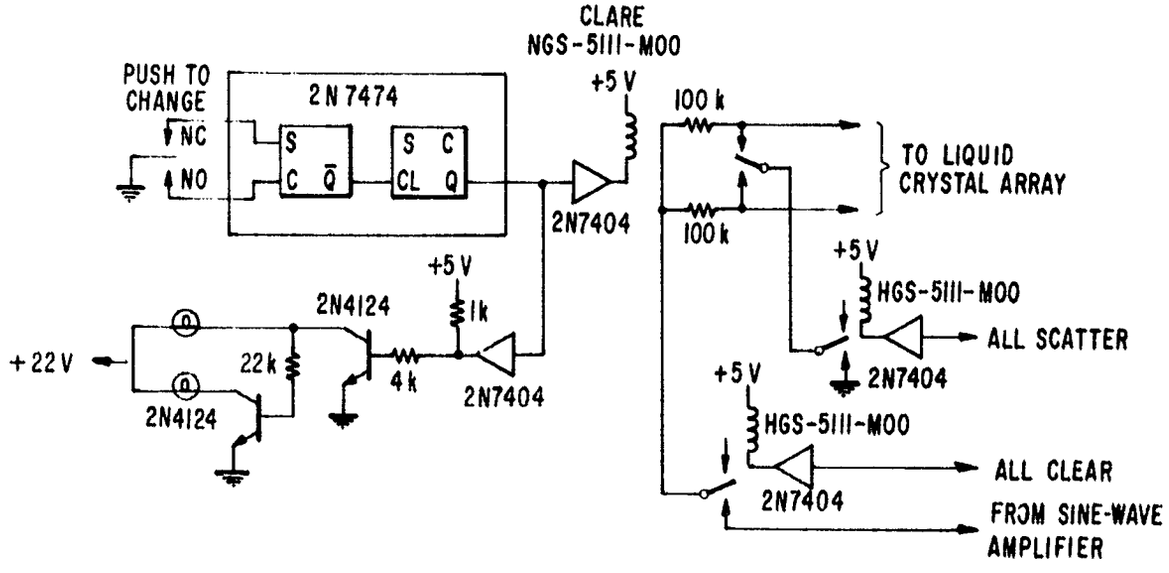

Figure 33. Circuit for one pair of liquid crystal elements.

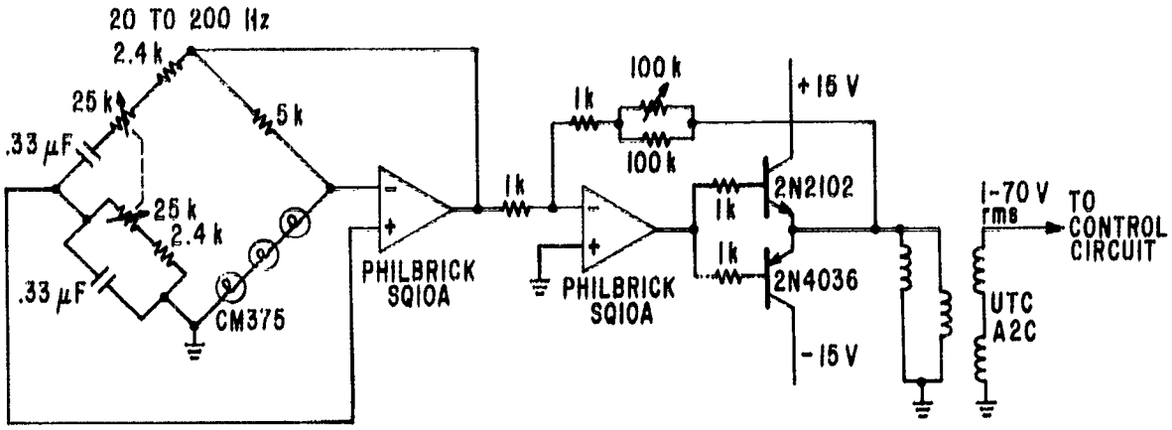

Figure 34. Drive circuit for liquid crystal excitation.

at the transformer secondary with amplitude control from 1 V rms to 70 V rms. The frequency is adjustable from 20 Hz to 200 Hz, with observable distortion present only at the lower frequencies, 20 Hz to 25 Hz, and at the higher voltages, 60 V to 70 V.

C. Storage Medium

Generation of the timing pulses which control the storage medium during writing (heat, corona, and also the Pockel cell polarization switch) is accomplished within one unit. Page heater selection and pulsing is performed within the main chassis, Fig. 35. High-voltage power supplies for the corona discharge and the polarization switch are separate (Fig. 36). A block diagram of the unit is given in Fig. 37, along with two alternative timing sequences for a write cycle in Fig. 38. Sequence A is used to write a hologram while the thermoplastic is fluid following an erase pulse of heat. In sequence B, the hologram is first erased. After cooling, the photoconductor-thermoplastic sandwich is sequentially charged, exposed, and recharged. A final heat pulse completes the recording sequence.

A write cycle is initiated (a) internally, by depressing the START button, or (b) externally, by the receipt of a ground signal from the external control console. Either event is stored within the control logic block of Fig. 37. This circuitry disables all the input gates and enables the output gates of the pulse circuits. Also, the state of the mode and sequence switches is locked in. These actions reduce the possibility of spurious signals operating the high-voltage circuits and, in turn, reduce the shock hazard. Upon completion of a cycle, the control logic is reset and a new command can be accepted.

The signals generated by the pulse circuits are:

(1) The page composer command enables the page composer control unit for the duration of the write cycle.

(2) The polarization command activates the power supply driving the polarization switch.

(3) Heat pulses for erasing and writing have widths adjustable from 0.1 to 15 msec.

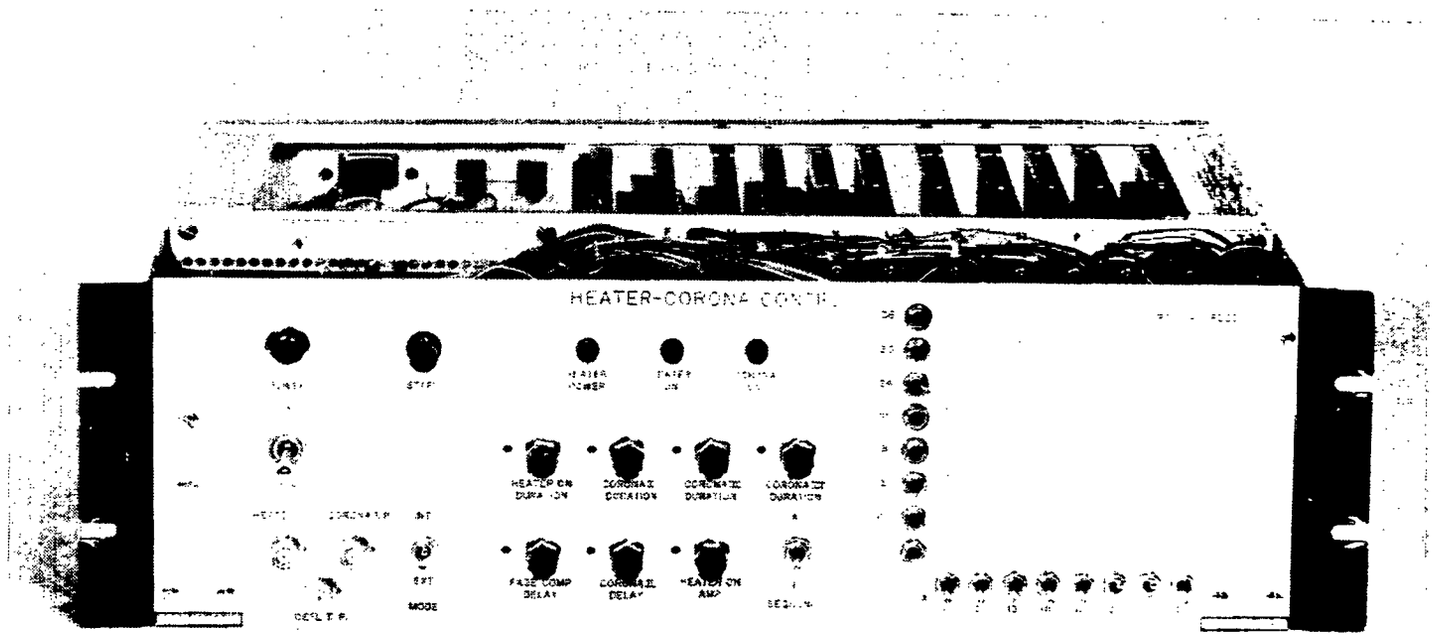

Figure 35. Storage medium control unit.

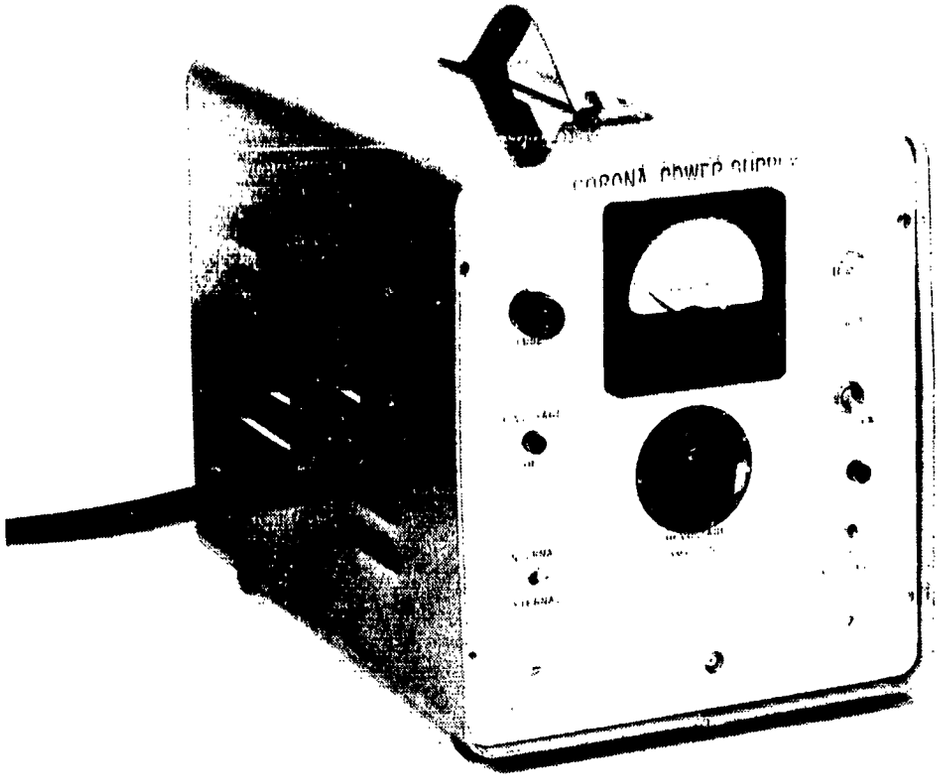

Figure 36. High voltage corona supply.

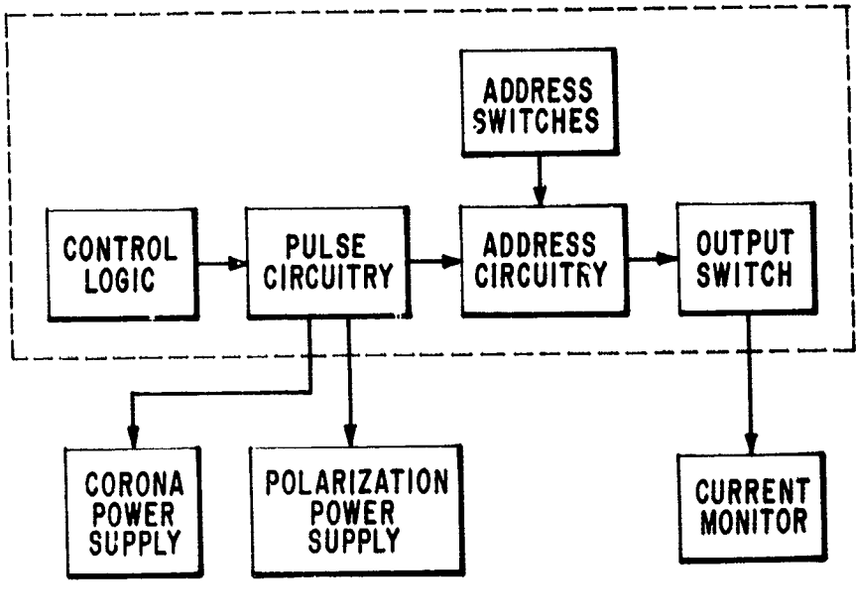

Figure 37. Block diagram of storage medium control unit.

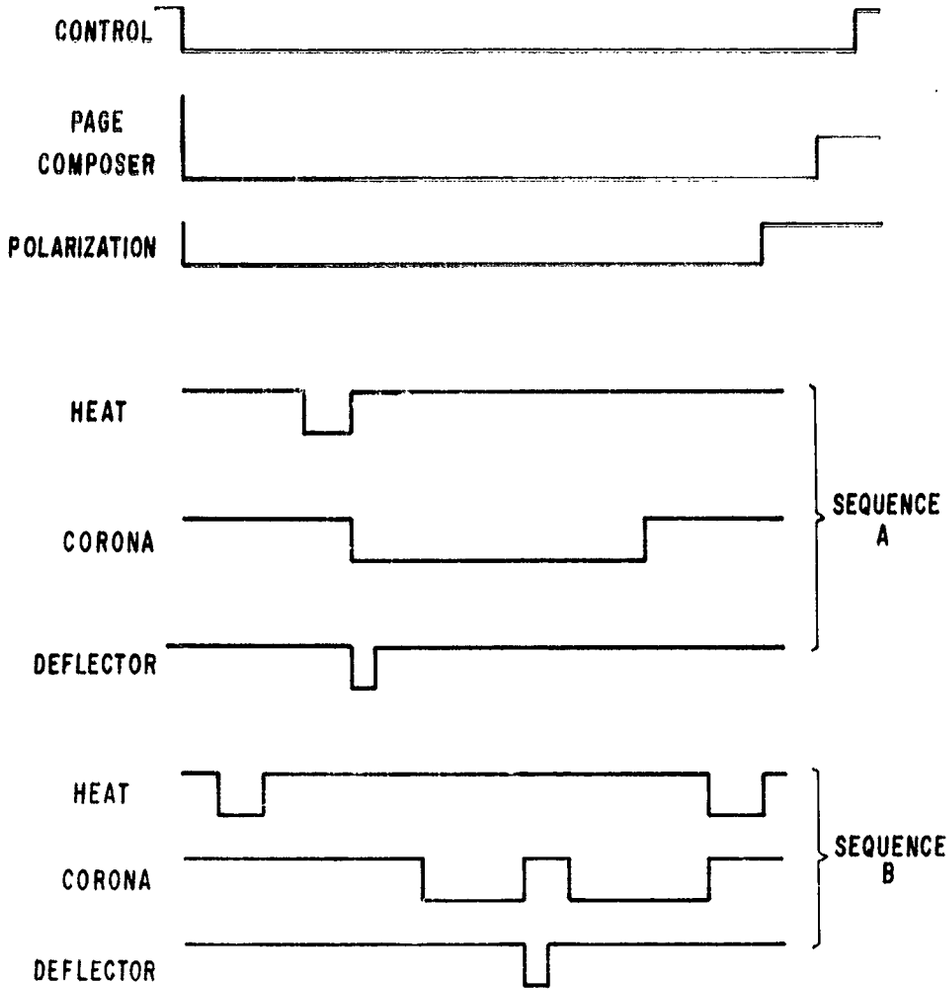

Figure 38. Timing sequences for a write cycle.

(4) Corona command durations are adjustable from 0.5 to 5 sec.

(5) The deflector command is a 1-msec pulse which starts the laser deflector control unit.

A page heater is addressed by one x- and one y-address switch. This results in the selection of one of the 48 heater drivers (Fig. 39) under control of the erase and write pulses. Connection is made to the memory plane with a 50-wire cable (48 pages, ground, power supply). The presence of write current is sensed and amplified. Currents larger than 10 mA light the HEAT POWER indicator. The peak value of the write current pulse is stored and is available at a back panel jack.

D. Detection System

During read, the image is detected by PIN photodiodes. The resulting electrical signals from each bit are then amplified, demodulated, integrated, and stored in parallel. The appropriate lamps on the

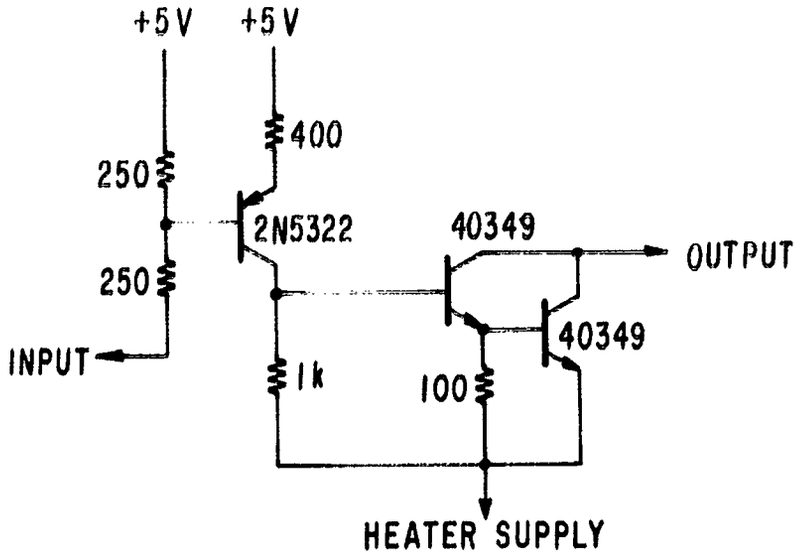

Figure 39. Driver circuit for a page heater.

front panel (see Fig. 40) are illuminated to indicate the detected information. Figure 41 shows the photodetector array and the preamplifiers.

A functional diagram of the detection system appears in Fig. 42. The light striking each diode is about 10^{-10} W peak, producing a current of 2×10^{-11} A peak. With an input impedance to the preamplifier of 5×10^{5} Ω, a signal voltage consisting of 3-msec pulses of 10 μV/pk amplitude is produced. The equivalent input noise voltage for the preamplifier is about 1 μV rms and its bandwidth is 2 kHz centered at the carrier frequency of 100 kHz. The voltage gain is × 5000.

Each stored bit consists of two spots, one illuminated and one opaque. The storage of "1" and "0" depends upon which spot is illuminated. Since two photodetectors connected differentially detect the light from these two spots, common mode illumination and electrical noise are attenuated. The 100-kHz sense signal leaves the preamplifier at a level of about 0.05 V peak and a relative phase angle of 0° or 180° depending upon whether the information is "1" or "0". It is further amplified and fed to a balanced demodulator which synchronously demodulates the 100-kHz signal into 3-msec pulses whose polarity is determined by the phase of the 100-kHz carrier relative to the local 100-kHz oscillator.

This demodulated signal is then integrated, with each 3-msec pulse increasing the output of the integrator while the incoherent noise is attenuated relative to the signal. The number of pulses to be integrated is selected by the "strobe delay" control, in effect increasing the sensitivity of the detection system but also increasing the time required for detection. The demodulated and integrated signal is now applied to the appropriate latch and indicator lamp for display as "1" or "0". The timing pulses for the read mode are illustrated in Fig. 43.

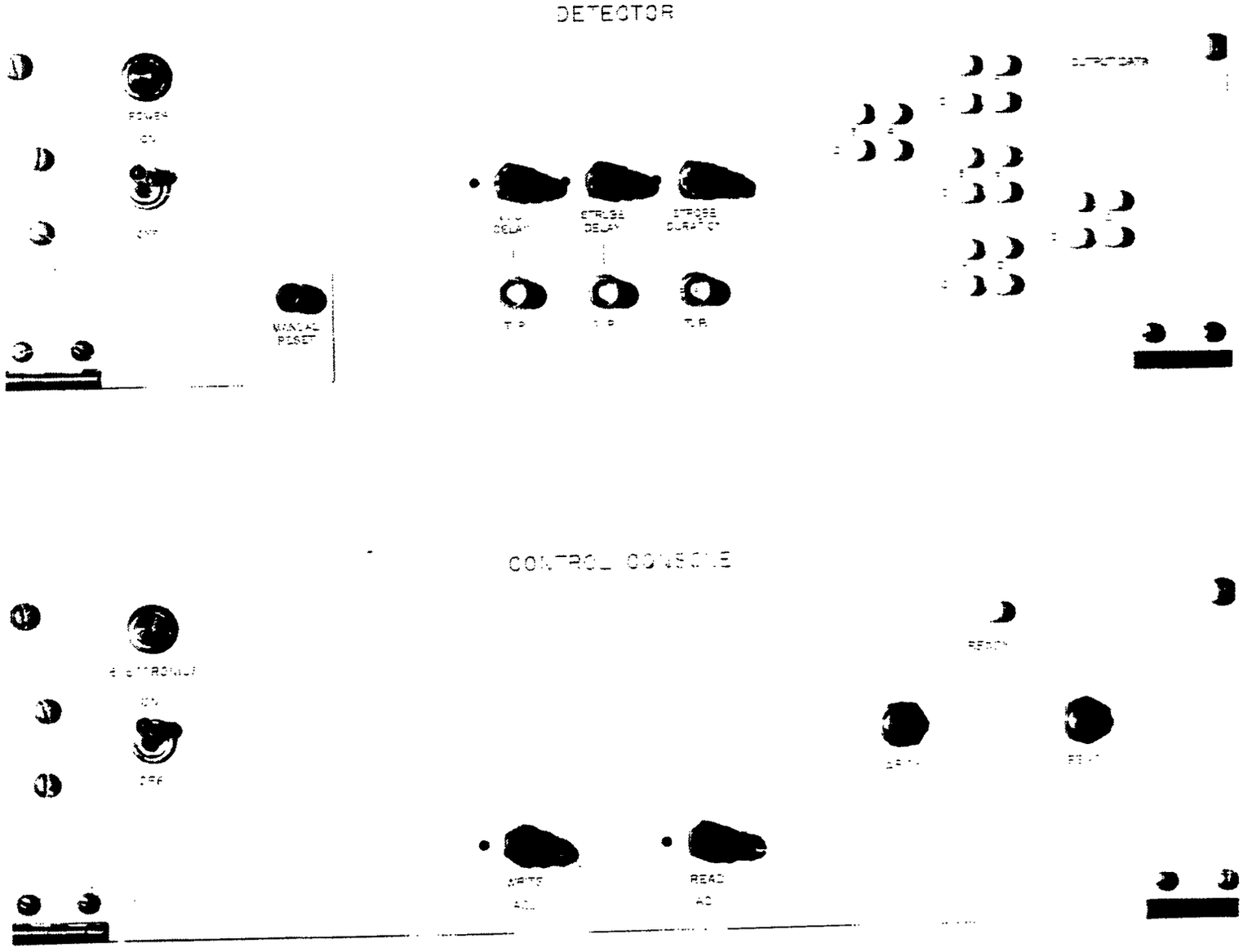

Figure 40. Front panels of the detection system unit and the control console unit.

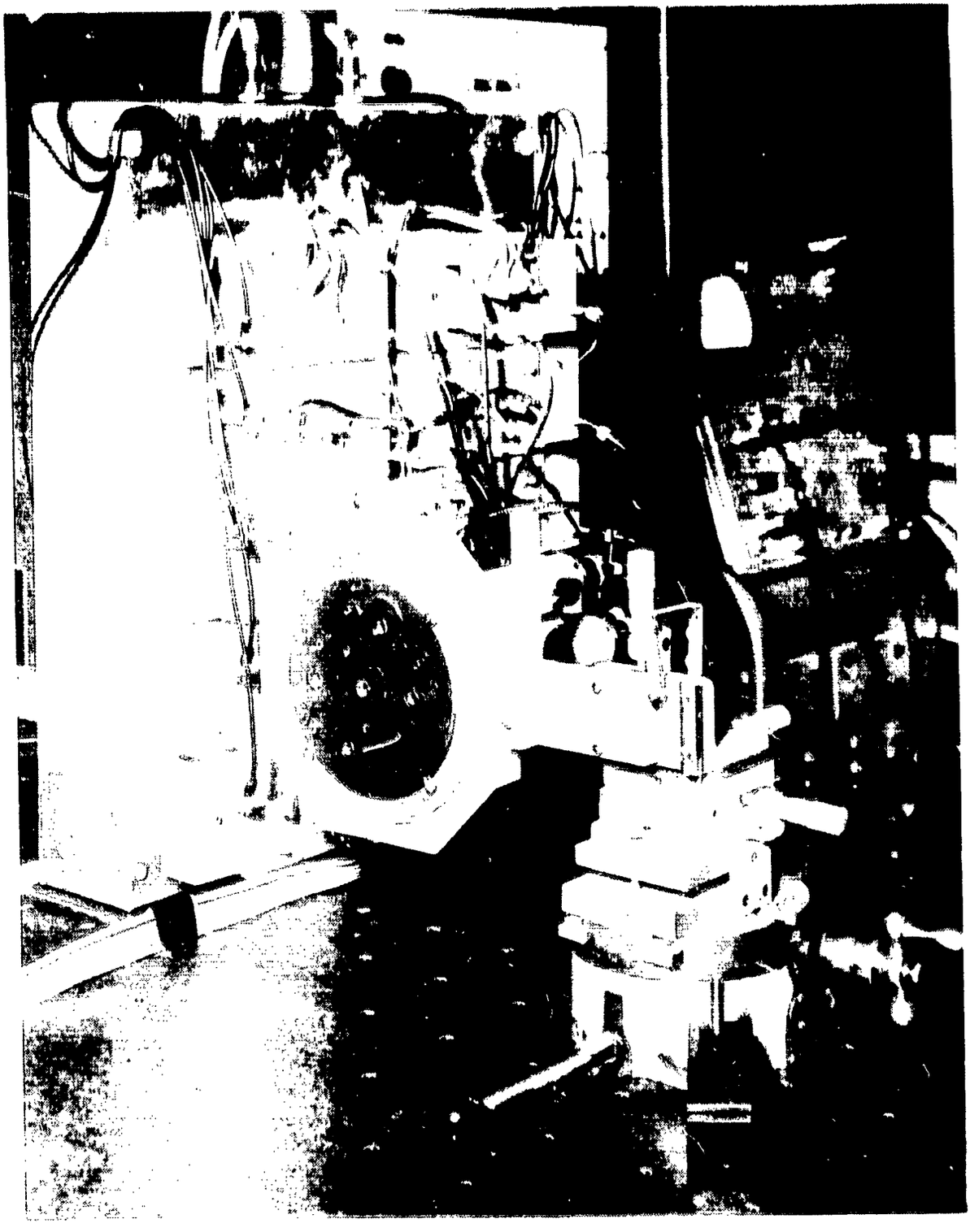

Figure 41. Photodetector array and preamplifiers.

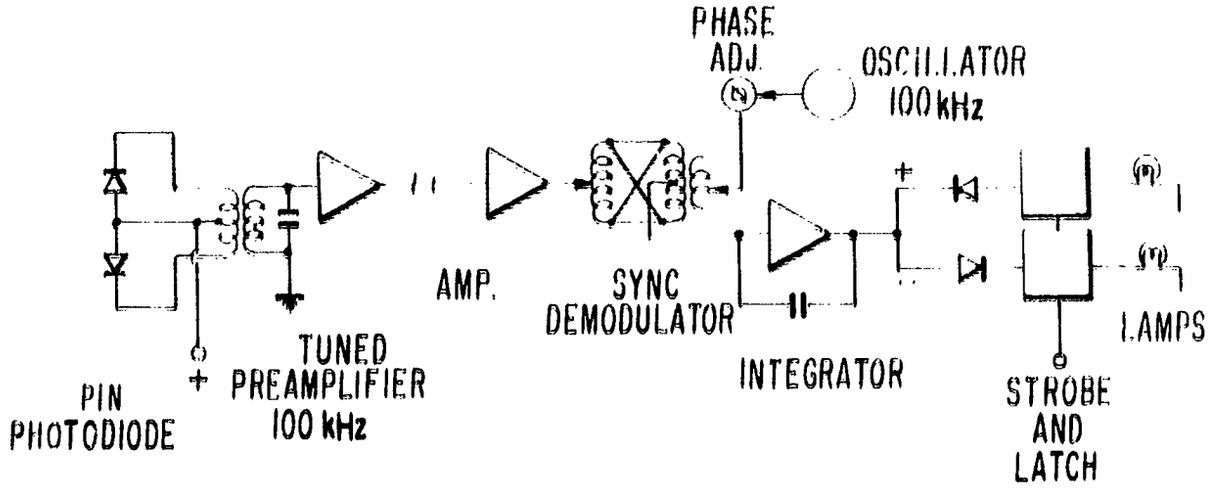

Figure 42. Detection system diagram.

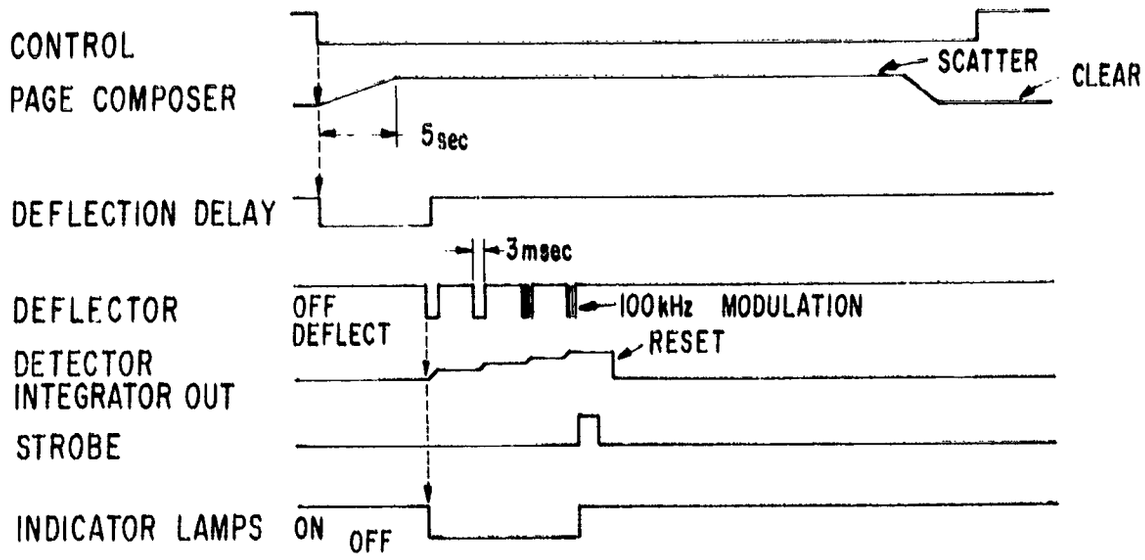

Figure 43. Timing sequence for reading.

E. Control Console

The control console, shown in Fig. 40, can be used to initiate the complete writing or reading sequence of the memory system. This chassis contains two pushbutton switches, one for reading and one for writing. Logic circuitry is present to prevent errors if either button is depressed before a cycle has been completed. Two monostable multivibrators generate control pulses whose widths are set to equal the duration of one complete read or write cycle.

IX. MEMORY SYSTEM OPERATION

Before the final assembly of the memory system, each of the major components was thoroughly tested alone and then in conjunction with others. The assembly procedure consisted of a step-by-step addition of each operating component. Completely successful operation of the memory system was achieved in accordance with the design objectives. Holograms were recorded and read out without error from all 48 active hologram locations, with no mechanical adjustments. The operating cycle with 300-mW laser output was: 2-sec corona charging time, 200-msec effective writing exposure duration, and 30-msec effective reading duration. Effective durations are listed because the temporal duty ratios of the laser beam are 0.1 for writing and 0.05 for reading.

We may extrapolate from the results of the partially populated system to conclude that a fully populated memory system of identical design would operate successfully. Replacement would be required only of the present aberrated deflector cells with ones displaying the full 40-spot Rayleigh resolution specified in the design.

The memory system is assembled on the surface of a 1.3-m by 4-m table that is vibration-isolated. Figure 44 shows a top view of the overall system with the approximate location of the components. The Frontispiece of this report is a photograph of the memory system with the photodetector array in the foreground, and the deflector system in the far background. The majority of the components are mounted on stages having precision adjustments, since tolerances are fractions of a milliradian for angles, and fractions of a millimeter for linear position. Vibration isolation supports are used between the table top and the argon laser head, which carries circulating cooling water. The strongest noise signals in the readout of an addressed hologram are contributed by spillover illumination from the reference beam hitting neighboring holograms, as expected from considerations discussed in the final design. When there is no hologram in the addressed location, partial readout of the information from the neighbors is detected. When a hologram is present at the addressed location, however, adequate rejection of the noise signals is obtained with the differential detection system.

As might be expected in a prototype system of this complexity, a number of engineering problems were encountered. Some of these have been alluded to in previous sections of this report; these discuss the trade-off considerations in the final design and the development of the various components. It was not practical, within the scope of this program, to ensure that the optimum performance was obtained in each component after the final assembly. Aberrations in the deflector cells, and lifetime problems with the laser, the dichromated gelatin hololens, the liquid crystal page composer, and the thermoplastic storage medium were all present. These factors represent the kinds of engineering details this program was intended to uncover, and to which increasing attention must be paid in programs to develop larger systems. The results of the present program demonstrate that these problems can be successfully attacked, and that the approach to high-capacity holographic storage systems which we have developed is soundly based.

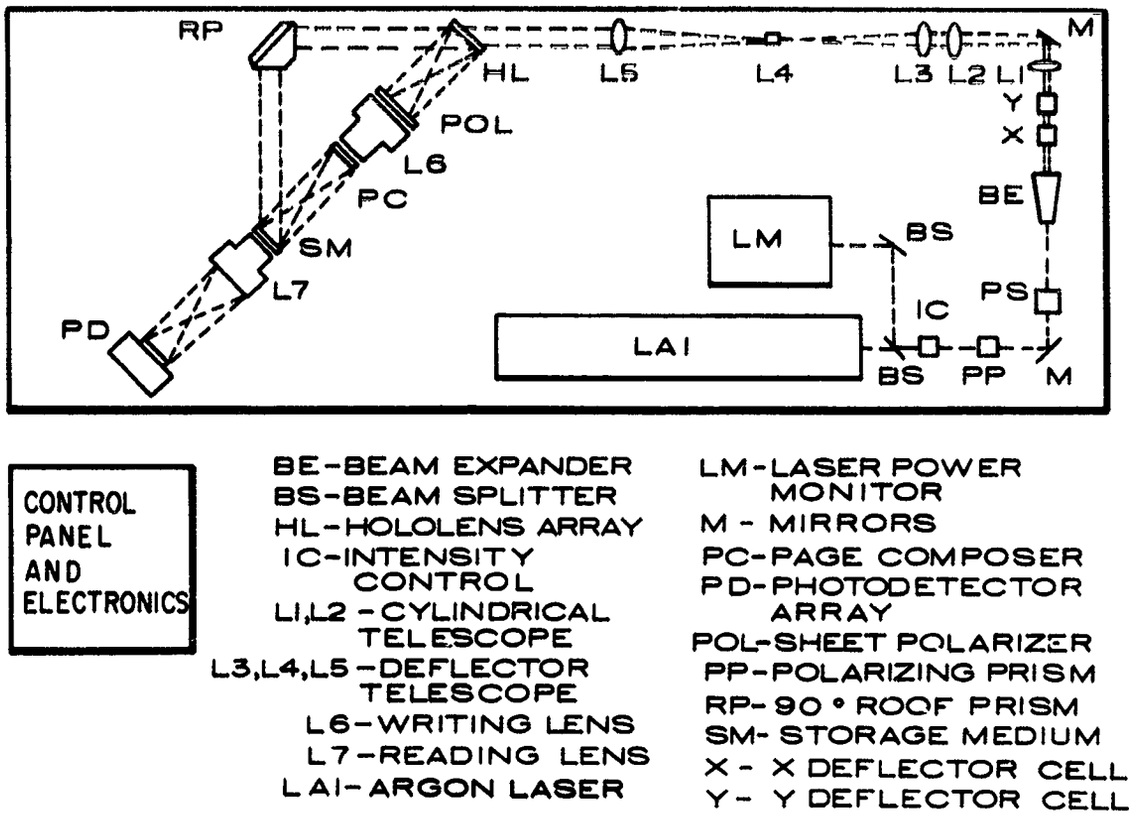

Figure 44. Approximate layout of optical memory system.

X. CONCLUSIONS

The following major conclusions are drawn from this program to develop a working prototype holographic read-write memory:

1. Practical design criteria have been established upon which to estimate the performance of a given configuration of components.

2. A working prototype system has been designed, constructed, and demonstrated.

3. For a given capacity and performance level, the trade-offs among component sizes can be quantitatively estimated. Criteria are proposed for optimizing the storage capacity, but have not been tested in a complete prototype system.

4. Future programs to develop larger-capacity memory systems must give increasing emphasis to engineering details such as tolerances, costs, and the practical performance limitations of the components.

REFERENCES

1. J. C. Urbach and R. W. Meier, "Thermoplastic Xerographic Holography," Appl. Opt. *5*, 666 (1966).

2. L. H. Lin and H. L. Beauchamp, "Write-Read-Erase in Situ Optical Memory Using Thermoplastic Holograms," Appl. Opt. *9*, 2088 (1970).

3. T. L. Credelle and F. W. Spong, "Thermoplastic Media for Holographic Recording," RCA Review *33*, 206 (1972).